



## Simulations of column-averaged CO<sub>2</sub> and CH<sub>4</sub> using the NIES TM with a hybrid sigma-isentropic ( $\sigma$ - $\theta$ ) vertical coordinate

D. A. Belikov<sup>1,2</sup>, S. Maksyutov<sup>1</sup>, V. Sherlock<sup>3</sup>, S. Aoki<sup>4</sup>, N. M. Deutscher<sup>5,6</sup>, S. Dohe<sup>7</sup>, D. Griffith<sup>6</sup>, E. Kyro<sup>8</sup>, I. Morino<sup>1</sup>, T. Nakazawa<sup>4</sup>, J. Notholt<sup>5</sup>, M. Rettinger<sup>9</sup>, M. Schneider<sup>7</sup>, R. Sussmann<sup>9</sup>, G. C. Toon<sup>10</sup>, P. O. Wennberg<sup>10</sup>, and D. Wunch<sup>10</sup>

<sup>1</sup>National Institute for Environmental Studies, Tsukuba, Ibaraki, Japan

<sup>2</sup>Division for Polar Research, National Institute of Polar Research, Tokyo, Japan

<sup>3</sup>Department of Atmospheric Research, National Institute of Water and Atmospheric Research, Wellington, New Zealand

<sup>4</sup>Center for Atmospheric and Oceanic Studies, Graduate School of Science, Tohoku University, Sendai, Japan

<sup>5</sup>Institute of Environmental Physics, University of Bremen, Bremen, Germany

<sup>6</sup>School of Chemistry, University of Wollongong, Wollongong, Australia

<sup>7</sup>IMK-ASF, Karlsruhe Institute of Technology (KIT), Karlsruhe, Germany

<sup>8</sup>Arctic Research Center, Finnish Meteorological Institute, Helsinki, Finland

<sup>9</sup>IMK-IFU, Karlsruhe Institute of Technology (KIT), Garmisch-Partenkirchen, Germany

<sup>10</sup>Department of Earth Science and Engineering, California Institute of Technology, Pasadena, CA, USA

Correspondence to: D. Belikov (dmitry.belikov@nies.go.jp)

Received: 15 November 2011 – Published in Atmos. Chem. Phys. Discuss.: 23 March 2012

Revised: 5 January 2013 – Accepted: 18 January 2013 – Published: 15 February 2013

**Abstract.** We have developed an improved version of the National Institute for Environmental Studies (NIES) three-dimensional chemical transport model (TM) designed for accurate tracer transport simulations in the stratosphere, using a hybrid sigma-isentropic ( $\sigma$ - $\theta$ ) vertical coordinate that employs both terrain-following and isentropic parts switched smoothly around the tropopause. The air-ascending rate was derived from the effective heating rate and was used to simulate vertical motion in the isentropic part of the grid (above level 350 K), which was adjusted to fit to the observed age of the air in the stratosphere. Multi-annual simulations were conducted using the NIES TM to evaluate vertical profiles and dry-air column-averaged mole fractions of CO<sub>2</sub> and CH<sub>4</sub>. Comparisons with balloon-borne observations over Sanriku (Japan) in 2000–2007 revealed that the tracer transport simulations in the upper troposphere and lower stratosphere are performed with accuracies of ~5% for CH<sub>4</sub> and SF<sub>6</sub>, and ~1% for CO<sub>2</sub> compared with the observed volume-mixing ratios. The simulated column-averaged dry air mole fractions of atmospheric carbon dioxide (XCO<sub>2</sub>) and methane (XCH<sub>4</sub>) were evaluated against daily ground-based high-resolution Fourier Transform Spectrometer (FTS) observations measured at twelve sites of the

Total Carbon Column Observing Network (TCCON) (Bialystok, Bremen, Darwin, Garmisch, Izaña, Lamont, Lauder, Orleans, Park Falls, Sodankylä, Tsukuba, and Wollongong) between January 2009 and January 2011. The comparison shows the model's ability to reproduce the site-dependent seasonal cycles as observed by TCCON, with correlation coefficients typically on the order 0.8–0.9 and 0.4–0.8 for XCO<sub>2</sub> and XCH<sub>4</sub>, respectively, and mean model biases of ±0.2% and ±0.5%, excluding Sodankylä, where strong biases are found. The ability of the model to capture the tracer total column mole fractions is strongly dependent on the model's ability to reproduce seasonal variations in tracer concentrations in the planetary boundary layer (PBL). We found a marked difference in the model's ability to reproduce near-surface concentrations at sites located some distance from multiple emission sources and where high emissions play a notable role in the tracer's budget. Comparisons with aircraft observations over Surgut (West Siberia), in an area with high emissions of methane from wetlands, show contrasting model performance in the PBL and in the free troposphere. Thus, the PBL is another critical region for simulating the tracer total column mole fractions.

## 1 Introduction

Carbon dioxide (CO<sub>2</sub>) and methane (CH<sub>4</sub>) are the greenhouse gases that contribute the most to global warming (IPCC, 2007). Recent studies of global sources and sinks of greenhouse gases, and their concentrations and distributions, have been based mainly on in situ surface measurements (GLOBALVIEW-CH<sub>4</sub>, 2009; GLOBALVIEW-CO<sub>2</sub>, 2010). The diurnal and seasonal “rectifier effect”, the covariance between surface fluxes and the strength of vertical mixing, and the proximity of local sources and sinks to surface measurement sites all have an influence on the measured and simulated concentrations, and complicate the interpretation of results (Denning et al., 1996; Gurney et al., 2004; Baker et al., 2006).

In contrast, the vertical integration of mixing ratio divided by surface pressure, denoted as the column-averaged dry-air mole fraction (DMF; denoted XG for gas *G*) is much less sensitive to the vertical redistribution of the tracer within the atmospheric column (e.g. due to variations in planetary boundary layer (PBL) height) and is more directly related to the underpinning surface fluxes than are near-surface concentrations (Yang et al., 2007). Thus, column-averaged measurements and simulations are expected to be very useful for improving our understanding of the carbon cycle (Yang et al., 2007; Keppel-Aleks et al., 2011; Wunch et al., 2011).

The Short-Wave InfraRed (SWIR) measurements from the SCIAMACHY imaging spectrometer onboard the ENVISAT satellite (Bovensmann et al., 1999) and the Japanese Greenhouse gases Observing SATellite (GOSAT) (Yokota et al., 2009) show some usefulness in determining the dry-air column-averaged mole fractions of carbon dioxide (XCO<sub>2</sub>) and methane (XCH<sub>4</sub>) (Bergamaschi et al., 2007, 2009; Bloom et al., 2010). However, the GOSAT retrieval algorithms are under continuing development and require reliable data for evaluation. One appropriate way to validate GOSAT is to use ground-based high-resolution Fourier Transform Spectrometer (FTS) observations from the Total Carbon Column Observing Network (TCCON) (Butz et al., 2011; Morino et al., 2011; Parker et al., 2011; Wunch et al., 2011). Ground-based FTS observations of the absorption of direct sunlight by atmospheric gases in the near-infrared (NIR) spectral region provide accurate measurements of the total columns of greenhouse gases (Wunch et al., 2010). Due to the limited number of TCCON sites, there is a relatively uneven spatial distribution of measurements, and measurements are not continuous because they depend on the cloud conditions (Wunch et al., 2011; Crisp et al., 2012). As a result, there are notable temporal and spatial gaps in the data coverage, particularly at high latitudes and over heavily clouded areas such as South America, Africa, and Asia; in such areas, model data can be used (Parker et al., 2011).

The synoptic and seasonal variabilities in XCO<sub>2</sub> and XCH<sub>4</sub> are driven mainly by changes in surface pressure, the tropospheric volume-mixing ratio (VMR) and the strato-

spheric concentration, which is affected in turn by changes in tropopause height. The effects of variations in tropopause height are more pronounced with increasing contrast between stratospheric and tropospheric concentrations; i.e., the influence is greater for CH<sub>4</sub> than for CO<sub>2</sub> due to CH<sub>4</sub> oxidation by OH, O(1D), and Cl in the stratosphere. A 30-ppbv change in tropospheric CH<sub>4</sub> or a 30-hPa change in tropopause height would produce a ~1.5 % variation in sea level XCH<sub>4</sub> (Washenfelder et al., 2003).

A precision of 2.5 ppm (better than 1 %) for CO<sub>2</sub> (Rayner and O'Brien, 2001) and 1%–2 % for CH<sub>4</sub> (Meirink et al., 2006) for monthly mean column-integrated concentrations on a regional scale is needed to reduce uncertainties in predictions of the carbon cycle. The target requirement formulated for the candidate Earth Explorer mission A-SCOPE mission is 0.02 Pg C yr<sup>-1</sup> per 106 km<sup>2</sup> or 0.1 ppm (Ingmann, 2009; Houweling et al., 2010). Transport-model-induced flux uncertainties that exceed the target requirement could also limit the overall performance of CO<sub>2</sub> missions such as GOSAT. However, the model accuracy requirement may depend on the measurement sensitivity (averaging kernel) for different tracers. If the measurement has little or no sensitivity to the tracer VMR in a given altitude region, then the accuracy of the model tracer concentrations in that region is irrelevant. A key element in accurately determining XCO<sub>2</sub> and XCH<sub>4</sub> is to obtain precise simulations of tracers throughout the atmosphere, including the stratosphere as well as the PBL.

Hall et al. (1999) suggested that many chemical transport models (CTMs) demonstrate some common failings of model transport in the stratosphere. The difficulty of accurately representing dynamical processes in the upper troposphere (UT) and lower stratosphere (LS) has been highlighted in recent studies (Mahowald et al., 2002; Waugh and Hall, 2002; Monge-Sanz et al., 2007). While there are many contributing factors, the principal factors affecting model performance in vertical transport are meteorological data and the vertical grid layout (Monge-Sanz et al., 2007).

The use of different meteorological fields in driving chemical transport models can lead to diverging distributions of chemical species in the upper troposphere/lower stratosphere (UTLS) region (Douglass et al., 1999). Several studies based on multi-year CTM simulations have shown that vertical winds directly supplied from analyses can result in an over-prediction of the strength of the stratospheric circulation and an under-prediction of the age of air (Chipperfield, 2006; Monge-Sanz et al., 2007). On the isentropic grid, the diabatic heating rate can be substituted for the analysed vertical velocity. A radiation scheme or recalculated radiation data can be used to resolve some of the problems of vertical winds from assimilated data products. Weaver et al. (1993) found that the use of a radiative scheme for long-term simulations gave a better representation of the meridional circulation, compared with simulations using the analysed vertical winds.

The isentropic vertical coordinate system has notable advantages over other types of coordinate systems, such as height, pressure, and “sigma” (Arakawa and Moorthi, 1988; Hsu, 1990), due to its ability to minimize vertical truncation and the non-existence of vertical motion under adiabatic conditions, except for diabatic heating (Bleck, 1978; Kalnay, 2002). These advantages result in reduced finite difference errors in sloping frontal surfaces, where pressure or  $z$ -coordinates tend to have large errors associated with poorly resolved vertical motion. The implementation of an isentropic coordinate with a radiation scheme helps to avoid erroneous vertical dispersion and enables the accurate calculation of vertical transport in the UTLS region (Mahowald et al., 2002; Chipperfield, 2006).

The aim of this study is to develop a NIES TM version with an improved tracer transport simulation in the stratosphere by implementing a sigma-isentropic coordinate system with an air-ascending rate derived from the effective heating rate, in order to obtain a more accurate simulation of atmospheric CO<sub>2</sub> and CH<sub>4</sub> profiles, and corresponding column-averaged concentration. The remainder of the paper is organized as follows. The model modifications are described in Sect. 2, and Sect. 3 presents an evaluation of the modeled age of the air and a validation the CO<sub>2</sub>, CH<sub>4</sub>, and SF<sub>6</sub> vertical profiles by comparison against balloon-borne in situ observations in the stratosphere. Also examined is the model’s performance in reproducing the near-surface concentration and free-troposphere vertical profiles of CH<sub>4</sub>. XCO<sub>2</sub> and XCH<sub>4</sub> simulated by NIES TM are compared with daily FTS observations at twelve TCCON sites between January 2009 and January 2011. Finally, a discussion (Sect. 4) and conclusions (Sect. 5) are provided.

## 2 Model description

This section describes the formulation of the NIES model version (denoted NIES-08.1i) used in this paper. Belikov et al. (2011) described the main model features, such as the flux-form dynamical core with a third-order van Leer advection scheme, a reduced latitude–longitude grid, a horizontal flux-correction method (necessary for mass conservation) and turbulence parameterization. However, the present paper focuses on the recently incorporated hybrid sigma-isentropic vertical coordinate and a change in the meteorological dataset used to drive the model.

### 2.1 Sigma-isentropic vertical coordinate

Previous NIES transport model versions with sigma-pressure and hybrid sigma-pressure vertical coordinate systems do not fully accommodate chemical and dynamical processes in the stratosphere, which results in the model failing to reproduce vertical tracer profiles. To overcome this issue, one can use climatological values of CO<sub>2</sub> and CH<sub>4</sub> in the stratosphere

(Eguchi et al., 2010). However, this approach does not account for year-to-year VMR variation and can distort the meridional mass circulation in long-term simulations.

It was previously thought that because potential temperature under adiabatic motion is individually conserved, it could be used as an ideal vertical coordinate. However, in several studies that have been published since the first successful integration of hydrostatic equations in isentropic coordinates performed by Eliassen and Raustein (1968), a number of disadvantages have been revealed. Many of them relate to the fact that isentropes intersect the Earth’s surface. The combined hybrid vertical coordinate system consisted of the  $\theta$  coordinate in the free atmosphere (where the air motion is quasi-adiabatic) with a  $\sigma$  terrain-following system near the surface, which helps to avoid problems with the  $\theta$  vertical coordinate (Bleck, 1978).

Hence, we follow the general methodology of Hsu and Arakawa (1990) and Konor and Arakawa (1997), and use the  $\sigma$ - $\theta$  hybrid sigma-isentropic coordinate that is isentropic in the UTLS region but terrain-following in the free troposphere. The coordinates switch smoothly near the tropopause level, as follows:

$$\sigma = \begin{cases} \left( P + \frac{\Delta P}{(\zeta - \theta)} \Delta \theta \right) \frac{1}{P_S}, & \text{if } \theta \geq \theta_T, \\ 1 - \frac{(P_S - P)(1 - \sigma_\theta)}{(P_S - P_\theta)}, & \text{if } \theta < \theta_T; \end{cases} \quad (1)$$

where  $\zeta$  denotes the level of the sigma-isentropic grid as described in Table 1,  $P$  and  $P_S$  are atmospheric pressure and surface atmospheric pressure respectively,  $\theta = T (P_S / P)^{(R/c_p)}$  is potential temperature,  $T$  depicts temperature,  $R$  is the molar gas constant,  $c_p$  is the specific heat for a constant pressure,  $\sigma_\theta$  and  $P_\theta$  are “sigma” and pressure at the level  $\theta_T$ , respectively. We set  $\theta_T = 360$  K to ensure that isentropes do not intersect the Earth’s surface.

### 2.2 Simulation of upward motion in the stratosphere

To calculate vertical transport in the  $\theta$ -coordinate domain of the hybrid sigma-isentropic coordinate, we use precalculated heating rates. Unlike the SLIMCAT model, which has an embedded diagnostic radiation scheme to calculate heating rates (Chipperfield, 2006), the NIES model interpolates the climatological heating rate at every meteorology data update step (3 h) at every model cell of the sigma-isentropic grid using a 2-D monthly distribution of the atmospheric reanalysis heating rate (see Sect. 2.3).

The most problematic region in modelling vertical transport is a level around the tropopause transition region known as the Tropical Tropopause Layer (TTL). Radiative heating in the TTL is a result of heating from the absorption of infrared radiation by ozone and carbon dioxide, balanced by infrared cooling, mainly from water vapor (Thuburn and Craig, 2002). The level termed as the “stagnation surface” (Sherwood and Dessler, 2003) occurs where the total heating rate  $Q_{\text{total}} = 0$ , and is demarcated by net cooling below and net

**Table 1.** Levels of the vertical grid in the NIES TM model.

	H, km	$\sigma = P/P_s$	$\approx \Delta$ , m	$\zeta(\sigma - \theta$ gridlevels), K	Number of levels
Near-surface layer	0–2	1.0–0.795	250	–	8
Free troposphere	2–12	0.795–0.195	1000	–, 330, 350	10
Upper troposphere and stratosphere	12–40	0.195–0.003	1000	365, 380, 400, 415,	14
			2000	435, 455, 475, 500	
			–	545, 590, 665, 850, 1325, 1710	
Total levels:					32

heating above. The height of this transition level is almost constantly around  $\theta = 360$  K ( $\approx 15$  km, 125 hPa) (Gettelman et al., 2004; Folkins et al., 1999). There is some variability in the level of  $Q_{\text{total}} = 0$ ; e.g.,  $\pm 500$  m between different locations and seasons;  $\pm 400$  m for individual profiles (Gettelman et al., 2004).

Among other aspects of Troposphere-to-Stratosphere Transport (TST) that are not adequately addressed, it is unclear how air parcels overcome the vertical gap between the main convective outflow around 350 K and the level with significant heating rates (Konopka et al., 2007). In some models, erroneous spurious meteorology, a diffusive numerical scheme (Eluszkiewicz et al., 2000), or extra vertical motion due to the implementation of vertical transport misrepresenting the adiabatic conditions are responsible for extra artificial mixing in this region, thereby obscuring the vertical transport problem.

In isentropic coordinates, the impact of such erroneous effects is significantly reduced. As a result, the use of a simulated heating rate leads to insufficient TST of tracers through the TTL. When models are unable to resolve a process explicitly, it is necessary to implement a parameterization to improve the simulation. Thus, Konopka et al. (2007) showed that more realistic tracer distributions are obtained by implementing the mixing parameterisation into a Chemical Lagrangian Model of the Stratosphere (CLaMS) with an isentropic vertical coordinate. Induced vertical mixing, driven mainly by vertical shear in the tropical flanks of subtropical jets, has been cited in explaining the upward transport of trace species from the main convective outflow to the tropical tropopause around 380 K (Konopka et al., 2007).

The total diabatic heating rates of different reanalysis products can produce dissimilar results (Fueglistaler et al., 2009). In our work, we implemented a scheme with additional transport in the TTL by increasing the air-ascending rate in the TTL, which was adjusted to fit the observed age of air in the stratosphere, as follows:

- For levels above 360 K (isentropic part of the vertical coordinate), the air-ascending rate was multiplied by 2.5.

- Constant vertical wind component ( $0.6 \text{ K day}^{-1}$ ) was set at the levels 180–40 hPa for tropical areas ( $15^\circ \text{ S} - 15^\circ \text{ N}$ ).

### 2.3 Meteorological data and vertical resolution

NIES TM is an off-line model driven by Japanese reanalysis data covering more than 30 years from 1 January 1979 (Onogi et al., 2007). The period of 1979–2004 is covered by the Japanese 25-year Reanalysis (JRA-25), which is a product of the Japan Meteorological Agency (JMA) and the Central Research Institute of Electric Power Industry (CRIEPI). After 2005, a real-time operational analysis, employing the same assimilation system as JRA-25, has been continued as the JMA Climate Data Assimilation System (JCDAS). The JRA-25/JCDAS dataset is distributed on Gaussian horizontal grid T106 ( $320 \times 160$ ) with 40 hybrid  $\sigma$ -p levels. The 6-hourly time step of JRA-25/JCDAS is coarser than the 3-hourly data from the National Centers for Environmental Prediction (NCEP) Global Forecast System (GFS) and Global Point Value (GPV) datasets, which were used in the previous model version (Belikov et al., 2011). However, with a better vertical resolution (40 levels on a hybrid  $\sigma$ -p grid versus 25 and 21 pressure levels for GFS and GPV, respectively) it is possible to implement a vertical grid with 32 levels (versus 25 levels used before), resulting in a more detailed resolution of the boundary layer and UTLS region (Table 1).

The 2-D monthly distribution of the climatological heating rate used to calculate vertical transport in the  $\theta$ -coordinate domain of the hybrid sigma-isentropic coordinate is prepared from JRA-25 reanalysis data, which are provided as the sum of short- and long-wave components on pressure levels.

### 2.4 Turbulent diffusion and deep convection parameterization

The calculation of turbulent diffusion is similar to that described by Maksyutov et al. (2008). To separate the transport processes in the well-mixed near-surface layer and free troposphere, we used 3-hourly PBL height data taken from European Centre for Medium-Range Weather Forecasts

(ECMWF) Interim Re-Analysis. Above the top of the PBL, the parameterisation of the turbulent diffusivity follows the approach used by Hack et al. (1993), who estimated free-troposphere diffusivity from local stability as a function of the Richardson number. Below the top of the PBL, the turbulent diffusivity is set to a constant value of  $40 \text{ m}^2 \text{ s}^{-1}$ , under the assumption that the boundary layer is well mixed.

Following Grell (1993), to simulate deep convection we used a Kuo-type penetrative cloud convection scheme including entrainment and detrainment processes on convective updrafts and downdrafts, as proposed by Tiedtke (1989). We calculated cumulus mass-flux from the detailed distribution of convection precipitation, using the method developed by Austin and Houze (1973), as first adopted by Feichter and Crutzen (1990). This approach is based on the fact that the amount of lifting air in an updraft core of a cumulus cell is related to precipitation, which it produces, and that the temperature excess and entrainment are reflected in its vertical development. Given the amount of the convective precipitation rate provided by the JRA-25/JCDAS dataset, the mass of air transported upward within the cells was computed from the conservation of moisture.

## 2.5 Model setup

In this paper, the performance of the new CTM in various configurations is investigated by running a series of experiments to study atmospheric tracer transport and the model's ability to reproduce the column-averaged dry air mole fractions of atmospheric CO<sub>2</sub> and CH<sub>4</sub>. The model was run at a horizontal resolution of  $2.5^\circ \times 2.5^\circ$  and 32 vertical levels from the surface to 3 hPa, using three tracers: CO<sub>2</sub>, CH<sub>4</sub>, and sulfur hexafluoride (SF<sub>6</sub>).

Forward model simulations were performed for SF<sub>6</sub> and CH<sub>4</sub> for 22 years (January 1988 to February 2011) using the simulation setup, initial distribution, fluxes, sinks, and chemical reactions (for CH<sub>4</sub>) described in the Protocol for TransCom-CH<sub>4</sub> inter-comparison (Patra et al., 2011). For the CH<sub>4</sub> simulation, an inverse model-adjusted flux was used, obtained by optimising the surface fluxes of CH<sub>4</sub> using the LMDZ model for the period 1988–2005 (Bousquet et al., 2006). For the 2006–2011 fluxes, the average seasonal cycle was repeated. For the SF<sub>6</sub> simulation for the period 1988–2005, the annual mean SF<sub>6</sub> emission distributions at  $1^\circ \times 1^\circ$  were taken from the Emission Database for Global Atmospheric Research (EDGAR, version 4.0) (<http://edgar.jrc.ec.europa.eu>), and the global totals were scaled by Levin et al. (2010). The 2005 distribution was used from 2006 onwards (Patra et al., 2011).

The simulation was started on 1 January 1988 using the initial 3D tracer distributions. This was prepared following a 10-year spin-up simulation by the Atmospheric General Circulation Model (AGCM)-based chemistry transport model with CH<sub>4</sub> and SF<sub>6</sub> concentrations at the South Pole of 1655 ppb and 1.95 ppt, respectively (Patra et al., 2011).

The CO<sub>2</sub> simulation was started on 1 January 2000 with the initial distribution derived from GLOBALVIEW-CO<sub>2</sub> (2010) observations using prescribed fluxes from the Comprehensive Observation Network for Trace gases by AirLiner (CONTRAIL) Transport Model Intercomparison (TMI) (Niwa et al., 2011), as follows:

1. Fossil fuel emissions are derived from the EDGAR-1998 distribution (Olivier and Berdowski, 2001) and the emission totals are scaled using the growth rate of the top 20 country-specific fossil fuel consumptions, as obtained from the Carbon Dioxide Information Analysis Center (CDIAC) (Boden et al., 2009).
2. The climatological inversion flux represents all non-fossil source/sink distributions over land and ocean, derived by inverse modelling with 12 TransCom3 models (Gurney et al., 2004) and from observational data obtained from GLOBALVIEW-CO<sub>2</sub> at 87 sites during 1999–2001 (Miyazaki et al., 2008).

## 3 Results

The current model version has been used in several tracer transport studies and was evaluated through participation in transport model intercomparisons (Niwa et al., 2011; Patra et al., 2011). The model results of tracer transport simulations show good consistency with observations and other models in the near-surface layer and in the free troposphere. However, the model performance in the UTLS region has not been evaluated in detail.

### 3.1 Validation of the mean age of air in the stratosphere

The mean age of air is purely a transport diagnostic. Modellers are ultimately interested in accurately simulating the distribution of trace gases that are affected by both transport and photochemistry (Waugh and Hall, 2002). The accurate determination of the chemical constituents that are transported across the tropopause, which are strongly affected by synoptic-scale events and other small-scale mixing processes, is a major challenge for modern CTMs (Hall et al., 1999). In the stratosphere, the vertical transport of substances is very weak due to the almost adiabatic conditions. However, many models are unable to reproduce sufficiently weak transport, especially in the tropical lower stratosphere, because the model grid does not reflect the underlying constraint that the flow is almost isentropic, making the model transport vulnerable to numerical errors (Mahowald et al., 2002). Generally, models tend to have ages of air in the stratosphere that are too young and tend to propagate the signal upward from the troposphere into the lower stratosphere too quickly, especially in the tropics (Hall et al., 1999; Park et al., 1999). By implementing a hybrid sigma-isentropic vertical coordinate, the observed age of air is more accurately

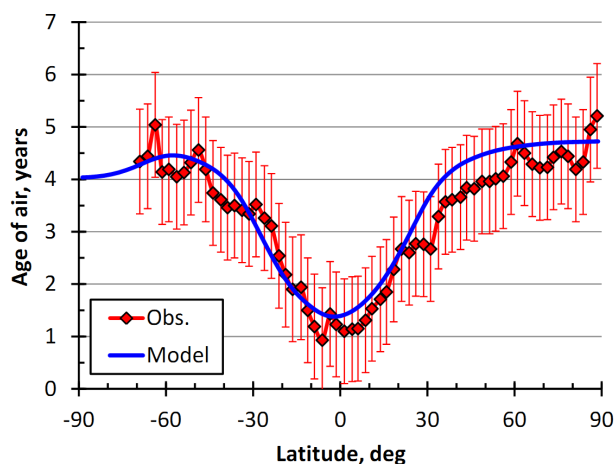


**Fig. 1.** Mean age of air at 20 km altitude from NIES TM simulations (blue line), compared with the mean age of air derived from in situ ER-2 aircraft observations of CO<sub>2</sub> (Andrews et al., 2001) and SF<sub>6</sub> (Ray et al., 1999) (red line). Error bars for the observations are  $2\sigma$  (Monge-Sanz et al., 2007).

determined than when using a model that employs a hybrid pressure grid (Mahowald et al., 2002; Chipperfield, 2006; Monge-Sanz et al., 2007).

The mean age of air can be calculated from measured or modelled tracer concentrations that are conserved and that vary linearly with time (Waugh and Hall, 2002). Among several chemical species that approximately satisfy the criterion of linear variation, CO<sub>2</sub> and SF<sub>6</sub> are the most reliable compounds with which to derive the mean age, because they are very long-lived species and their annual mean concentrations have been increasing approximately linearly (Conway et al., 1994; Maiss et al., 1996). In spite of uncertainties due to non-linearity in tropospheric growth rates and the neglect of photochemical processes (Waugh and Hall, 2002), estimates performed with CO<sub>2</sub>, SF<sub>6</sub>, and other tracers show rather good agreement.

In this paper, SF<sub>6</sub> is simulated to derive the mean age of the air in the upper troposphere and in the lower stratosphere. The model was run for 22 years before the simulation results were analysed, because the age of stratospheric air was unchanged for the last 30 years (Engel et al., 2009).

Figure 1 shows the annual mean of the zonal-mean age of air obtained with NIES TM at an altitude of 20 km, together with the mean age values derived from CO<sub>2</sub> and SF<sub>6</sub> ER-2 aircraft observations (Andrews et al., 2001). Both the model and observation estimations of the mean age indicate values of approximately 1 year near the equator, large gradients in the subtropics, and values of around 4–5 years at high latitudes.

The vertical profiles of mean age derived from in situ measurements of CO<sub>2</sub> and SF<sub>6</sub> show that at all latitudes, the mean age of the air increased monotonically with height through-

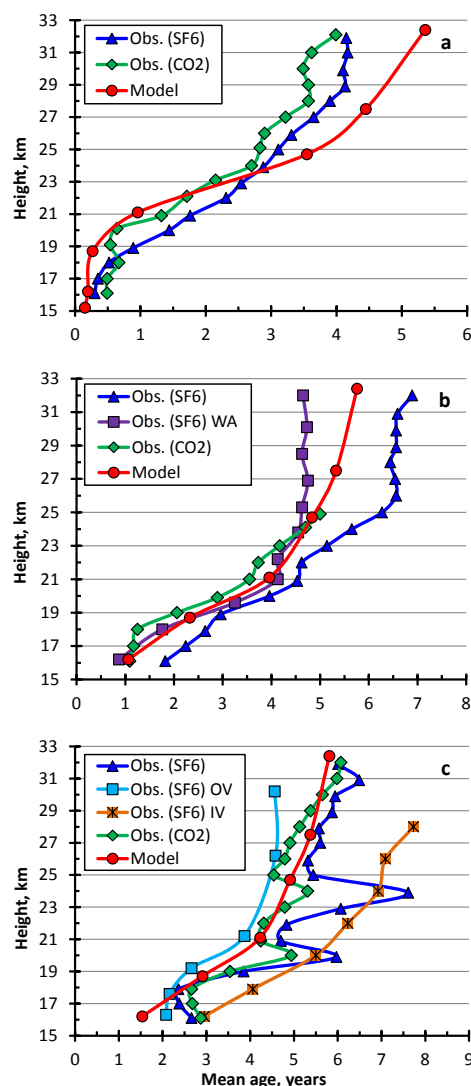


**Fig. 2.** Comparison of observed and modelled (red lines) mean age of air at latitudes of: (a) 5° S, (b) 40° N, and (c) 65° N. The lines with symbols represent observations: in situ SF<sub>6</sub> (dark blue line with triangles) (Elkins et al., 1996; Ray et al., 1999), whole air samples of SF<sub>6</sub> (purple line with squares for (b) panel, light blue line with squares outside vortex and orange line with asterisks inside vortex (c) panel) (Harnisch et al., 1999), and mean age from in situ CO<sub>2</sub> (green line with diamonds) (Boering et al., 1996; Andrews et al., 2001).

out the stratosphere, with only weak vertical gradients above 25 km (Fig. 2). The model slightly overestimated the age of air in the tropics (Fig. 2a) and underestimated it at middle and high latitudes (Fig. 2b, c). The spikes in high-latitude profiles (Fig. 2c) are due to the sampling of fragments of polar vortex air. Despite this, the general shape of the isopleths in Fig. 3 is realistic and illustrates the balance of the meridional mass (Brewer–Dobson) circulation, which tends to increase latitu-

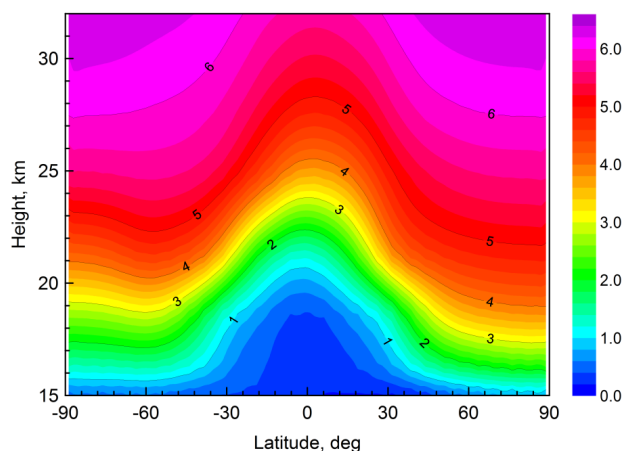


**Fig. 3.** Cross-Sections of the annual mean age of air (years) from NIES TM simulations of SF<sub>6</sub> with JRA-25/JCDAS reanalysis.

dinal slopes, and isentropic mixing, which tends to decrease the slopes (Plumb and Ko, 1992).

### 3.2 Validation of CO<sub>2</sub>, CH<sub>4</sub>, and SF<sub>6</sub> vertical profiles in the stratosphere

To evaluate the model's ability to reproduce stratospheric transport, the simulated vertical profiles of CO<sub>2</sub>, CH<sub>4</sub>, and SF<sub>6</sub> were analysed and compared against balloon-borne observation data (Fig. 4). The observed VMRs were derived from six individual profiles of balloon-borne measurements performed by Takakiyo Nakazawa and Shuhji Aoki (Tohoku University) for Sanriku, Japan (39.17° N, 141.83° E) for 28 August 2000, 30 May 2001, 4 September 2002, 6 September 2004, 3 June 2006, and 4 June 2007, following the procedures described by Nakazawa et al. (2002). The vertical profiles were determined by averaging the modelled and observed concentrations taken for the same day and time. The error bars show the standard deviation. To calculate the mean profiles, we subtracted the annual growth rate of 0.23 pptv yr<sup>-1</sup> (Stiller et al., 2008) for SF<sub>6</sub> and variable growth rates derived by Conway and Tans (2011) for CO<sub>2</sub> for the period 2001–2007. No correction is applied to the CH<sub>4</sub> concentration, because a slowdown in the CH<sub>4</sub> increase was observed in the stratosphere for the period 1978–2003 (Rohs et al., 2006).

In general, the NIES TM is able to capture the shape of a tracer's vertical profile in the stratosphere. These profiles consist of several parts with different properties, such as: (1) weak gradients up to 70 hPa; (2) a large decrease of VMRs at heights between 70 and 50 hPa; (3) almost constant concentrations from 50 to 30 hPa, and (4) significant (especially for CH<sub>4</sub>) gradients from 30 hPa upwards (Fig. 4).

The modelled profile of SF<sub>6</sub> is consistent with the observed profile up to 50 hPa and has a relatively large (~5 %) positive bias above this level (Fig. 4a). SF<sub>6</sub> is a chemically

inert tracer (in the troposphere and stratosphere), indicating that transport alone is responsible for the variation in its profile. The discrepancy between the observed and simulated vertical profiles is consistent with the underestimation of the age of air above 40 hPa in temperate and high-latitude zones, as discussed above.

In contrast, the CH<sub>4</sub> profile was found to have a strong negative bias (~5 %) between 100 and 20 hPa (Fig. 4b), which disappeared with height. It would appear that a change in the CH<sub>4</sub> loss rate due to chemical reactions leads to less excessive destruction of methane and better agreement with observations above 20 hPa. SF<sub>6</sub> is not involved in any chemical reactions to compensate for the extra vertical transport in the UTLS region.

The simulated CO<sub>2</sub> vertical profile (Fig. 4c) overestimated the observed profile by 0.5 % below 90 hPa and underestimated it by 0.5 % above 90 hPa. The individual profiles used to derive the average profile were obtained at the beginning and end of the vegetation season; consequently, the modelled CO<sub>2</sub> profile shows a seasonal variation at the 140–100 hPa level. The large error bars become smaller with height, enabling an estimate of the seasonal variation of approximately 1–2 ppmv at 140 hPa. The spread of data in the profiles at about 1.5 ppmv at all levels is common for measured CO<sub>2</sub>.

Thus, the simulated vertical profiles of CH<sub>4</sub> and SF<sub>6</sub> are generally within ~5 % of the observed VMRs, while CO<sub>2</sub> profiles are within 1 %. Given that the stratosphere only represents 15 %–20 % of the mid-latitude atmospheric column mass, these results are sufficient for this study. It is noted that the simulated CO<sub>2</sub> profiles have a smoother shape and show a better consistency with the observations, as the simulation was run for 9 years less than that for CH<sub>4</sub> and SF<sub>6</sub>. This result indicates the ability of the model to reproduce vertical profiles of the tracers in the lower stratosphere more accurately for a relatively short-term period (about 10 years) than for a long-term period (about 20 years). This result reflects the fact that the model tends to overestimate tracer concentrations in the uppermost part of the domain, due to sparse grid layers in the lower stratosphere.

### 3.3 Validation of CO<sub>2</sub>, CH<sub>4</sub>, and SF<sub>6</sub> concentrations in the free troposphere

The ability of the NIES TM to simulate SF<sub>6</sub> and CO<sub>2</sub> in the near-surface layer and in the free troposphere was validated by Belikov et al. (2011) and Niwa et al. (2011). The inter-hemispheric gradients of SF<sub>6</sub> and CO<sub>2</sub>, and vertical profiles and seasonal variations of CO<sub>2</sub> were evaluated against the GLOBALVIEW-CO<sub>2</sub> and World Data Centre for Greenhouse Gases (WDCGG) observations, and against an aircraft measurement dataset of CONTRAIL (Niwa et al., 2011). Although the NIES TM's performance in terms of transport, emission distribution and chemical loss, inter-hemispheric gradient, seasonal cycle, and synoptic variations in CH<sub>4</sub> were also quantified as part of the TransCom-CH<sub>4</sub> experiment

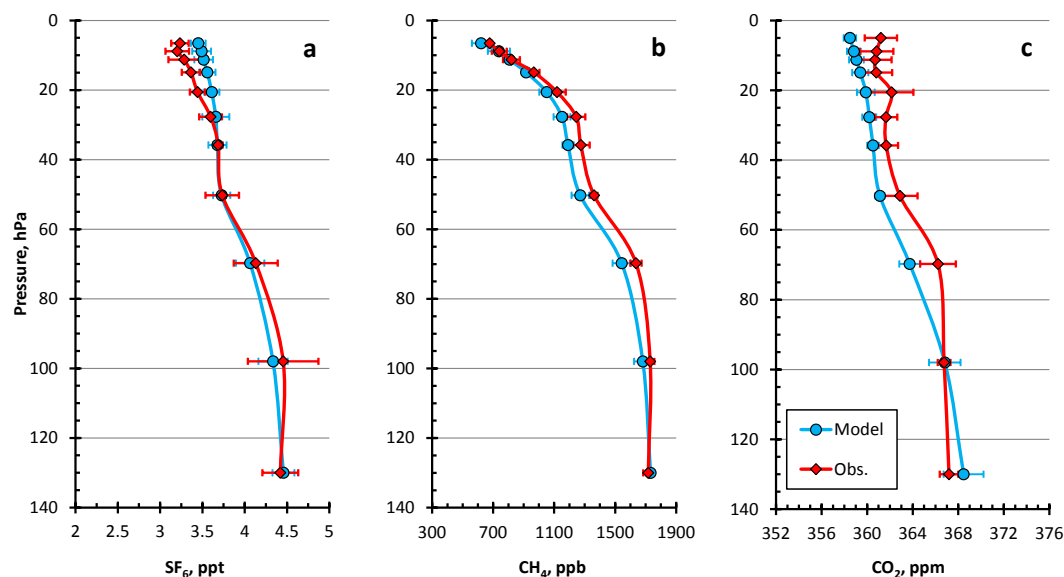


**Fig. 4.** Comparison of observed and modelled concentration averaged for the period 2000–2007: **(a)** SF<sub>6</sub>, **(b)** CH<sub>4</sub>, and **(c)** CO<sub>2</sub>. The observed VMRs were derived from six individual profiles of balloon-borne measurements over Sanriku, Japan (39.17° N, 141.83° E).

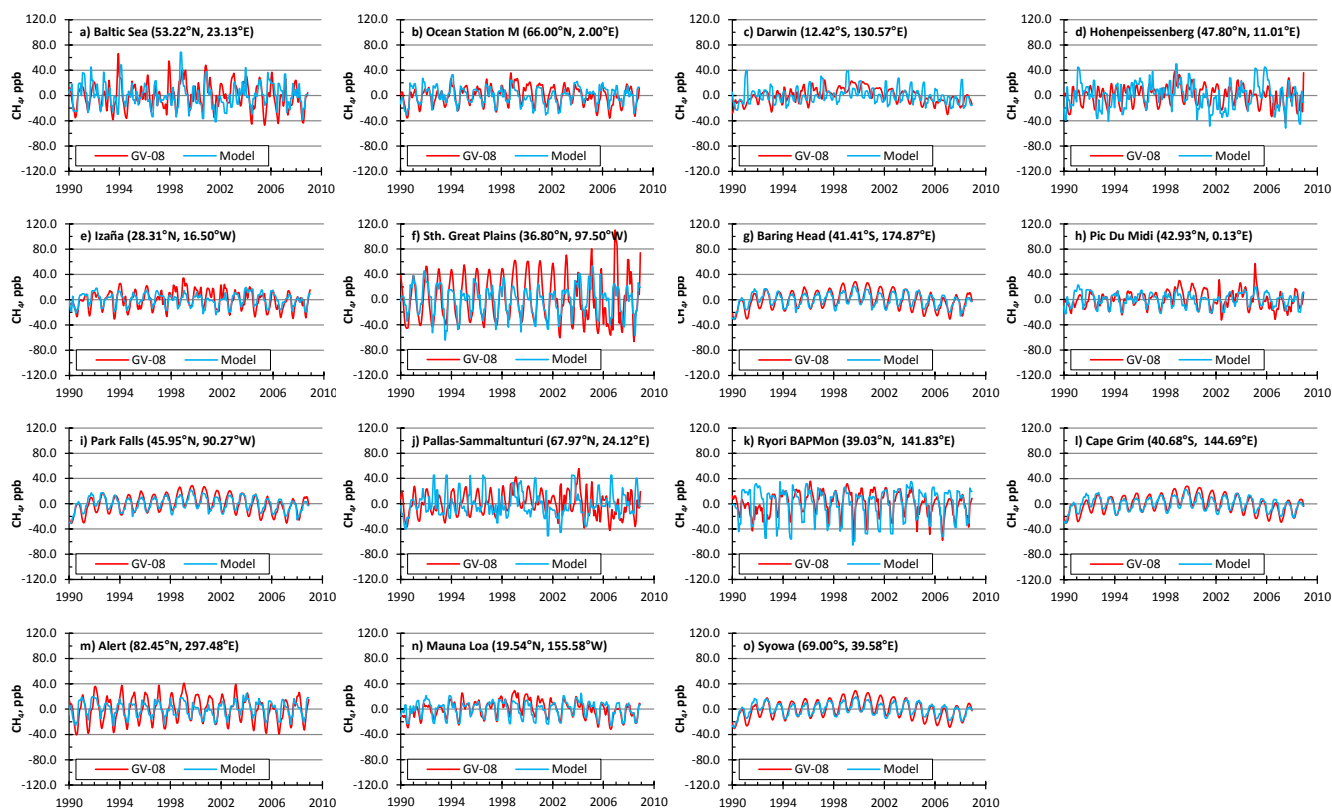


**Fig. 5.** Detrended seasonal cycle of surface CH<sub>4</sub> volume mixing ratio for GLOBALVIEW stations (corresponding TCCON stations in parentheses): **(a)** Baltik See (Bialystok); **(b)** Ocean Station M (Bremen); **(c)** Darwin (Darwin); **(d)** Hohenpeissenberg (Garmisch); **(e)** Izaña (Izaña); **(f)** Southern Great Plains (Lamont); **(g)** Baring Head Station (Lauder); **(h)** Pic Du Midi (Orleans); **(i)** Park Falls (Park Falls); **(j)** Pallas-Sammaltunturi (Sodankylä); **(k)** Ryori (Tsukuba); **(l)** Cape Grim (Wollongong); **(m)** Alert; **(n)** Mauna Loa; and **(o)** Syowa.

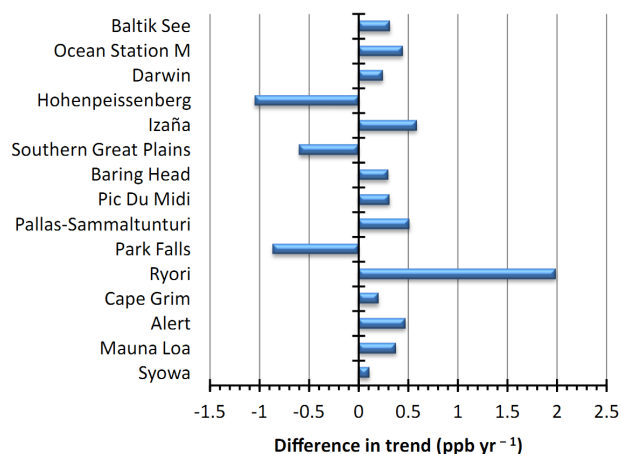


**Fig. 6.** Average difference between simulated and observed trends (ppb yr<sup>-1</sup>) of CH<sub>4</sub> for Jan 1990 and Dec 2009 at GLOBALVIEW stations.

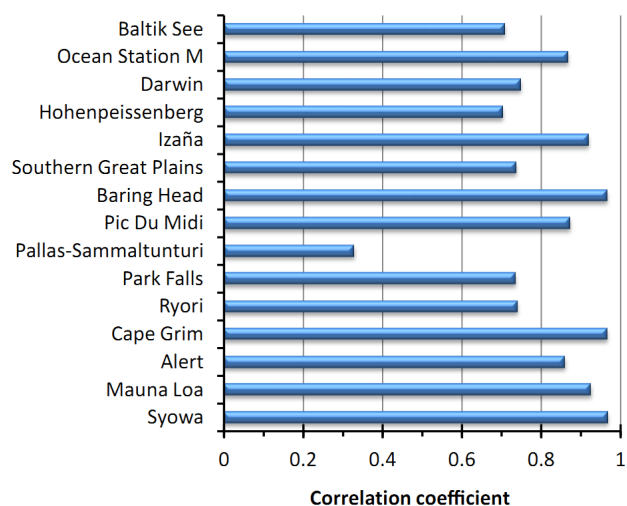


**Fig. 7.** Correlation coefficients between simulated and observed CH<sub>4</sub> at GLOBALVIEW stations.

(Patra et al., 2011), this section focuses on near-surface seasonal variations and vertical profiles of methane.

### 3.3.1 Validation of near-surface CH<sub>4</sub> concentrations

Given that one of the aims of this paper is to validate the modelled column-averaged concentration against ground-based FTS TCCON observations, we examined the variability of CH<sub>4</sub> concentrations at TCCON sites. We selected GLOBALVIEW-CH<sub>4</sub> (GV-CH<sub>4</sub>) sites located near to TCCON stations and the following three sites additionally: Alert (82.45° N, 62.52° W), Mauna Loa (19.53° N, 155.58° W), and Syowa (69.00° S, 39.58° E) (Table 2). Time-series plots of the modelled near-surface CH<sub>4</sub> concentrations were compared with in situ observation data. For simplicity, we refer to

the names of nearby TCCON stations with surface GV-CH<sub>4</sub> station data. Fig. 5 shows time series of the CH<sub>4</sub> seasonal cycle for 1990–2008, which was manually adjusted by the annual mean concentration at the South Pole.

The simulations indicate that the model underestimated the near-surface seasonal cycle at northern high-latitudes. The model bias for Alert was 13.0 ppb versus 8.4 and 6.5 ppb for Mauna Loa and Syowa, respectively. A similar feature was observed for the trend of CH<sub>4</sub>, for which the model bias decreased from the North Pole (0.5 ppb yr<sup>-1</sup>) to the South Pole (0.1 ppb yr<sup>-1</sup>) (Fig. 6).

Southern Australia and New Zealand are relatively isolated from large-scale CH<sub>4</sub> emission sources, and as a result there was some consistency between the modelled and measured values ( $r = 0.87$ – $0.9$  for Baring Head and Cape Grim) in capturing the small variability (amplitude of 30 ppb). As Darwin is located relatively close to the Asian tropics (Malaysia and Indonesia), which is marked by very high variations in CH<sub>4</sub> emissions and complicated meteorological conditions, the model was not able to reproduce the seasonal cycle as well at this site, compared with other sites.

The results for North America, whilst including a range of emission sources, indicated a similar agreement in the phase for Park Falls and Southern Great Plains (Lamont) ( $r \sim 0.7$ ) and performed poorly in reproducing the growth rate, as the model underestimated the trends for both sites (Fig. 6). Mixed results were also found for the European sites: good agreement with observations was found for Pic Du Midi (Orleans) and Ocean Station M (Bremen), but poor agreement for Hohenpiessenberg (Garmisch) and Pallas-Sammaltunturi (Sodankylä). However, the worst agreement in the growth rate was found for Ryori (Tsukuba), where the model systematically underestimated the seasonal variations of the tracer.

We found very different model performance at remote sites such as Ocean Station M (Bremen), Izaña, Cape Grim (Wollongong), Baring Head (Lauder), Alert, Mauna Loa, and Syowa, where the model was generally able to accurately reproduce the phase of variations in surface concentrations (correlation coefficients of 0.85–0.95). For other sites (Park Falls, Pallas-Sammaltunturi (Sodankylä), Ryori (Tsukuba), and Southern Great Plains (Lamont)), however, where multiple emission sources are located close by and where local meteorology plays a major role, the model encountered difficulties in reproducing the complicated CH<sub>4</sub> surface concentrations.

### 3.3.2 Validation of CH<sub>4</sub> vertical profiles in the troposphere

To examine the variability of CH<sub>4</sub> in the near-surface layer and in the free troposphere, the VMRs simulated by the model were compared against aircraft observations performed by T. Machida (NIES) in 1993–2007 over Surgut, West Siberia. This location is marked by high CH<sub>4</sub> emissions from wetlands.

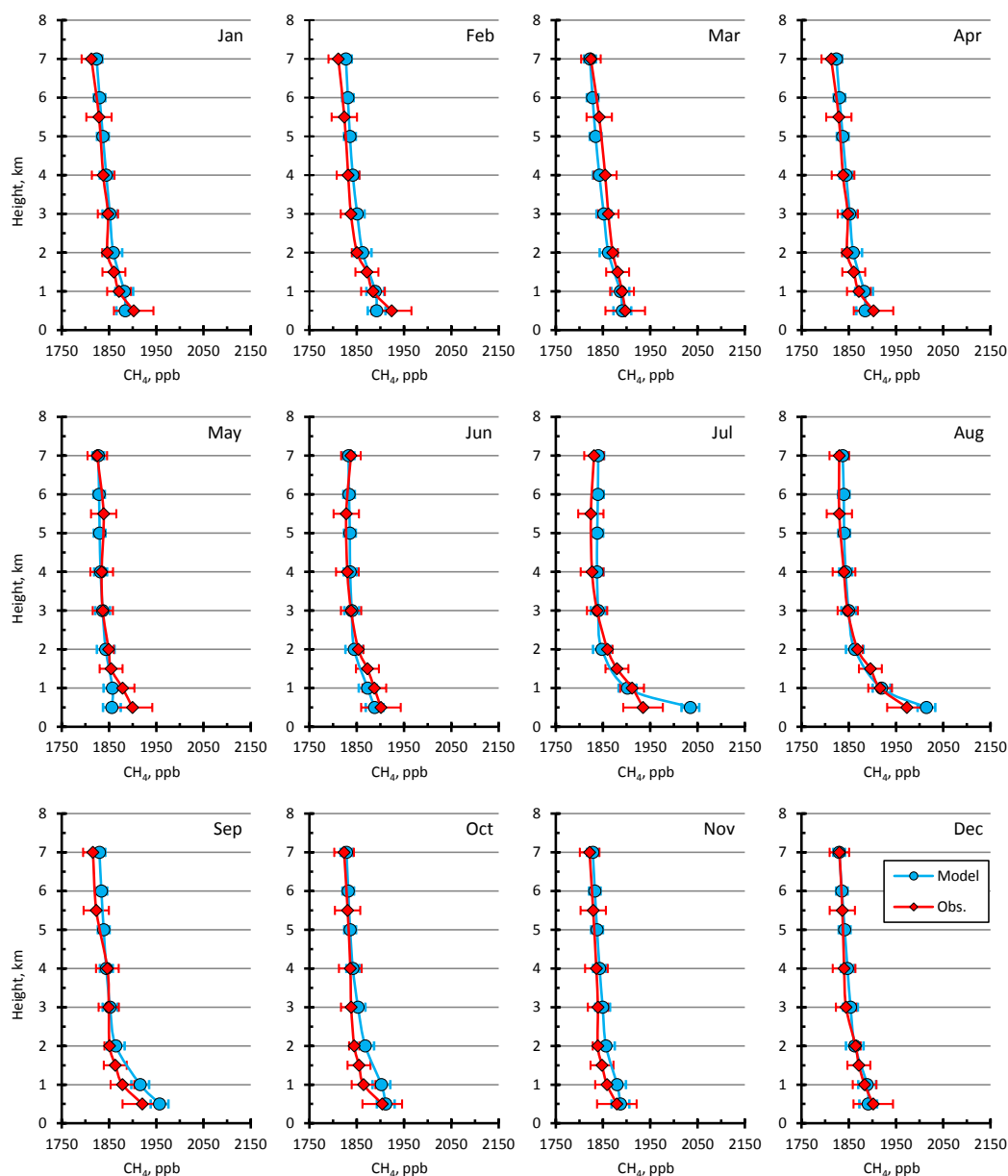


**Fig. 8.** Comparison of observed and modeled CH<sub>4</sub> concentrations averaged for the period 1993–2007 over Surgut, West Siberia. The vertical profiles were produced by averaging the modelled and observed concentrations taken on the same day and at the same time. Error bars show the standard deviation.

It is challenging to perform simulations of CH<sub>4</sub> in the northern high-latitude regions because of large uncertainties in emissions due to under-sampling of CH<sub>4</sub> concentrations over most regions, particularly where melting permafrost releases CH<sub>4</sub> (Zhuang et al., 2009). Despite this problem, the modelled and measured values are in good agreement above 1 km (Fig. 8). The model is less effective in reproducing the high variability in CH<sub>4</sub> concentrations in the near-surface layer and could not accurately simulate short-term variations. The VMR at the 1-km level and below was highly variable

due to changes in the PBL height, which determined the volume of air absorbing all emitted tracers and the local meteorology. The greatest amount of variability was found in July and August (Fig. 8), reflecting variations in the PBL height during the daytime and high emissions from wetlands.

The averaged trends derived from the biases for the levels at 1, 3, and 7 km show similar values in all cases, in the range about 40 ppb depending on the season (Fig. 9). This result indicates balanced transport from the surface layer to the free

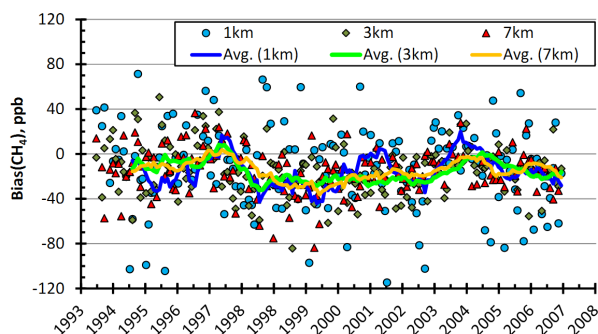


**Fig. 9.** Time series of model bias (modelled CH<sub>4</sub> concentration minus observed) and the averaged (moving average with period 12) value of the bias for the 1, 3, and 7 km levels over Surgut (61.25° N, 73.43° E) for the period 1993–2007.

troposphere due to the implementation of the JR-25/JCDAS meteorological data provided on the sigma-pressure levels.

The correlation coefficients between simulated and observed CH<sub>4</sub> values show an increase towards the free troposphere, from 0.19 for the 1-km level to 0.53 for the 7-km level, because vertical propagation decreases with height. While other factors are involved, changes in PBL height and associated variation in the rates of tracer redistribution from local sources to the free troposphere are important drivers of high variability in CH<sub>4</sub> VMR at GV-CH<sub>4</sub> sites with high emissions. Similar trends were obtained by Houweling et al. (2010) for four different transport models used to simulate XCO<sub>2</sub>.

### 3.4 Validation of CO<sub>2</sub> and CH<sub>4</sub> column-averaged DMFs

The main goal of this paper was to validate the model's ability to reproduce the CO<sub>2</sub> and CH<sub>4</sub> column-averaged dry-air mole fractions using observations from TCCON sites, which is a global network of ground-based high-resolution FTS recording direct solar spectra in the near-infrared spectral region (Wunch et al., 2011). The overall objectives of TCCON include improving our understanding of the carbon cycle and validating XCO<sub>2</sub> and XCH<sub>4</sub> retrieved from satellite observations.

For comparison, we selected simulated and TCCON XCO<sub>2</sub> and XCH<sub>4</sub> taken at around 13:00 ± 1 h local time over TCCON sites for the period January 2009 to January 2011. Samples within this time-frame were collected for analysis, to assess the model's performance within the GOSAT overpass interval. The following TCCON sites were selected: Bialystok (Poland, 53.22° N, 23.13° E); Bremen (Germany, 53.10° N, 8.85° E); Darwin (Australia, 12.42° S, 130.89° E); Garmisch (Germany, 47.48° N, 11.06° E); Izaña (Spain, 28.30° N, 16.50° W); Lamont (USA, 36.6° N, 97.49° W); Lauder (New Zealand, 45.04° S, 169.68° E); Orleans (France, 47.97° N, 2.11° E); Park Falls (USA, 45.95° N, 90.27° W); Sodankylä (Finland,

67.37° N, 26.63° E); Tsukuba (Japan, 36.05° N, 140.12° E); and Wollongong (Australia, 34.41° S, 150.88° E). For the Lauder site we used data from the 125HR spectrometer when available (February 2010–present) and data from the older 120HR spectrometer prior to February 2010.

To compare the modelled total column with measurements directly, it is necessary to consider the measurement averaging kernels. Averaging kernels describe the sensitivity of the retrieved total column to a perturbation in absorber abundance in a given layer of the vertical profile (Rodgers and Connor, 2003; Wunch et al., 2011). At present TCCON provides a single set of averaging kernels for CO<sub>2</sub> and CH<sub>4</sub>, tabulated as a function of solar zenith angle (SZA), based on a subset of retrievals from the Lamont site ([http://tcccon.ipac.caltech.edu/tcccon\\_aux\\_pub.html](http://tcccon.ipac.caltech.edu/tcccon_aux_pub.html)). Site-specific a priori profiles used in TCCON CO<sub>2</sub> retrievals were provided by each site PI. A single CH<sub>4</sub> a priori (independent of location and time) has been used in TCCON retrievals at all sites other than Darwin and Sodankylä. At these sites site-specific and time-independent CH<sub>4</sub> profiles are provided. The tabulated averaging kernels were interpolated to the SZA of the measurements and applied in the calculation of the CO<sub>2</sub> or CH<sub>4</sub> vertical column in accordance with Eq. (15) of Connor et al. (2008). The tracer vertical column abundances were then divided by the dry-air column abundance to calculate the column-averaged dry air mole fractions, denoted X<sub>y</sub> or DMF hereafter.

Due to the SZA dependence of the TCCON averaging kernels, the difference between total column concentrations calculated with and without averaging kernels is greatest for sites located farthest from the equator, Bialystok, Bremen and Sodankylä, which yield values in the range −0.6 to 2.0 ppm and −20 to 20 ppb for XCO<sub>2</sub> and XCH<sub>4</sub>, respectively; the difference is smallest for the tropical and subtropical sites Darwin and Izaña, with values of −0.4 to 0.4 ppm and −5.0 to 5.0 ppb, respectively.

Time series of the model results and FTS data for XCO<sub>2</sub> and XCH<sub>4</sub> are shown in Figures 10 and 12, respectively. These figures were produced by manually adjusting the XCO<sub>2</sub> and XCH<sub>4</sub> model offsets (2.2 ppm and −32.0 ppb, respectively). The offsets were caused by the use of slightly out-dated fluxes for the simulations, the implementation of an averaging kernel, and misfit in the modelled vertical profiles. Thus, a XCH<sub>4</sub> offset may also be induced due to high uncertainty of OH and other species, which are responsible for CH<sub>4</sub> destruction in the atmosphere.

Matching the model's mean CH<sub>4</sub> with the observations is achieved by adjusting either global total emissions or sinks, which both have large uncertainties (10–20%, Patra et al., 2011). Small residual offsets can be adjusted by tuning global emissions, but long-term simulations are required to reach equilibration between sources and sinks. Adding a small 30 ppb offset to simulated results is nearly equivalent to the corresponding proportional change in the emissions fields on

**Table 2.** Locations of TCCON and GLOBALVIEW stations used in the comparisons.

No.	TCCON stations			GLOBALVIEW stations			
	Station name	Lat.	Lon.	Station name	Lat.	Lon.	Alt., m
1	Bialystok	53.22° N	23.13° E	Baltik See	55.35° N	17.22° E	28
2	Bremen	53.10° N	8.85° E	Ocean Station M	66.00° N	2.00° E	5
3	Darwin	12.42° S	130.89° E	Darwin	12.42° S	130.57° E	3
4	Garmisch	47.48° N	11.06° E	Hohenpeissenberg	47.80° N	11.01° E	990
5	Izaña	28.30° N	16.50° W	Izaña	28.31° N	16.50° W	2360
6	Lamont	36.61° N	97.49° W	Southern Great Plains	36.80° N	97.50° W	374
7	Lauder	45.04° S	169.68° E	Baring Head	41.41° S	174.87° E	80
8	Orleans	47.97° N	2.11° E	Pic Du Midi	42.93° N	0.13° E	2877
9	Park Falls	45.95° N	90.27° W	Park Falls	45.95° N	90.27° W	483
10	Sodankylä	67.37° N	26.63° E	Pallas-Sammaltunturi	67.97° N	24.12° E	560
11	Tsukuba	36.05° N	140.12° E	Ryori BAPMon	39.03° N	141.83° E	260
12	Wollongong	34.41° S	150.88° E	Cape Grim	40.68° S	144.69° E	164
13				Alert	82.45° N	297.48° E	110
14				Mauna Loa	19.54° N	155.58° W	3397
15				Syowa	69.00° S	39.58° E	14

**Table 3.** Correlation coefficients and biases of the modelled XCO<sub>2</sub> and XCH<sub>4</sub>.

No.	Station name		XCO <sub>2</sub>		XCH <sub>4</sub>	
			Correlation	Bias, ppm	Correlation	Bias, ppb
1	Bialystok	(Poland, 53.22° N, 23.13° E)	0.93	0.61	0.74	4.52
2	Bremen	(Germany, 53.10° N, 8.85° E)	0.88	0.19	0.72	1.27
3	Darwin	(Australia, 12.42° S, 130.89° E)	0.90	−0.62	0.55	−2.41
4	Garmisch	(Germany, 47.48° N, 11.06° E)	0.93	0.76	0.44	0.98
5	Izaña	(Spain, 28.30° N, 16.50° W)	0.87	−0.53	0.53	9.05
6	Lamont	(USA, 36.61° N, 97.49° W)	0.91	−0.44	0.62	−1.13
7	Lauder	(New Zealand, 45.04° S, 169.68° E)	0.90	0.22	0.58	−1.20
8	Orleans	(France, 47.97° N, 2.11° E)	0.96	0.17	0.59	−8.80
9	Park Falls	(USA, 45.95° N, 90.27° W)	0.95	−0.28	0.51	−2.30
10	Sodankylä	(Finland, 67.37° N, 26.63° E)	0.94	1.21	0.40	20.91
11	Tsukuba	(Japan, 36.05° N, 140.12° E)	0.85	−0.24	0.53	3.80
12	Wollongong	(Australia, 34.41° S, 150.88° E)	0.80	0.32	0.66	−8.19
All stations			0.90	−0.62 (−0.16 %) 1.21 (0.31 %)	0.54	−8.80 (−0.49 %) 20.91 (1.16 %)

the order of 2 %. For CO<sub>2</sub>, the corresponding bias correction is about 0.5 %.

For TCCON, the observation symbols and error bars represent the mean and standard deviations of the weighted average if more than one measurement within the 13:00 ± 1 h local time was available. Note that gaps in the TCCON data time-series are due to cloud and instrumental issues.

### 3.4.1 Modelled XCH<sub>4</sub> compared with TCCON FTS observations

Reproducing the CH<sub>4</sub> seasonal variation was a big challenge, because of its rather small amplitude and high scatter relative to the mean climatological value. As expected, the seasonal variation in XCH<sub>4</sub> over the Southern Hemisphere (i.e.,

Darwin, Lauder, and Wollongong) was weak (Fig. 10a, g, h) due to the smaller contribution of the local emissions; consequently, the model's ability to reproduce the variation generally depends on reproducing of large-scale transport. The correlation coefficients for these sites are very similar (0.55, 0.58, and 0.66, respectively; Table 3).

In contrast, model performance at the Northern sites strongly depends on powerful local sources. The best correlation coefficients (in the range of 0.62–0.74) are obtained for Lamont, Bremen and Bialystok, where seasonal variation in XCH<sub>4</sub> has the highest amplitude. European sites show slightly large biases of 4.52, −8.80, and 20.91 for Bialystok, Orleans and Sodankylä, respectively. For Orleans, the correlation is rather weak (0.59, Table 3), whereas for the corresponding GLOBALVIEW station of Pic Du Midi it is rather

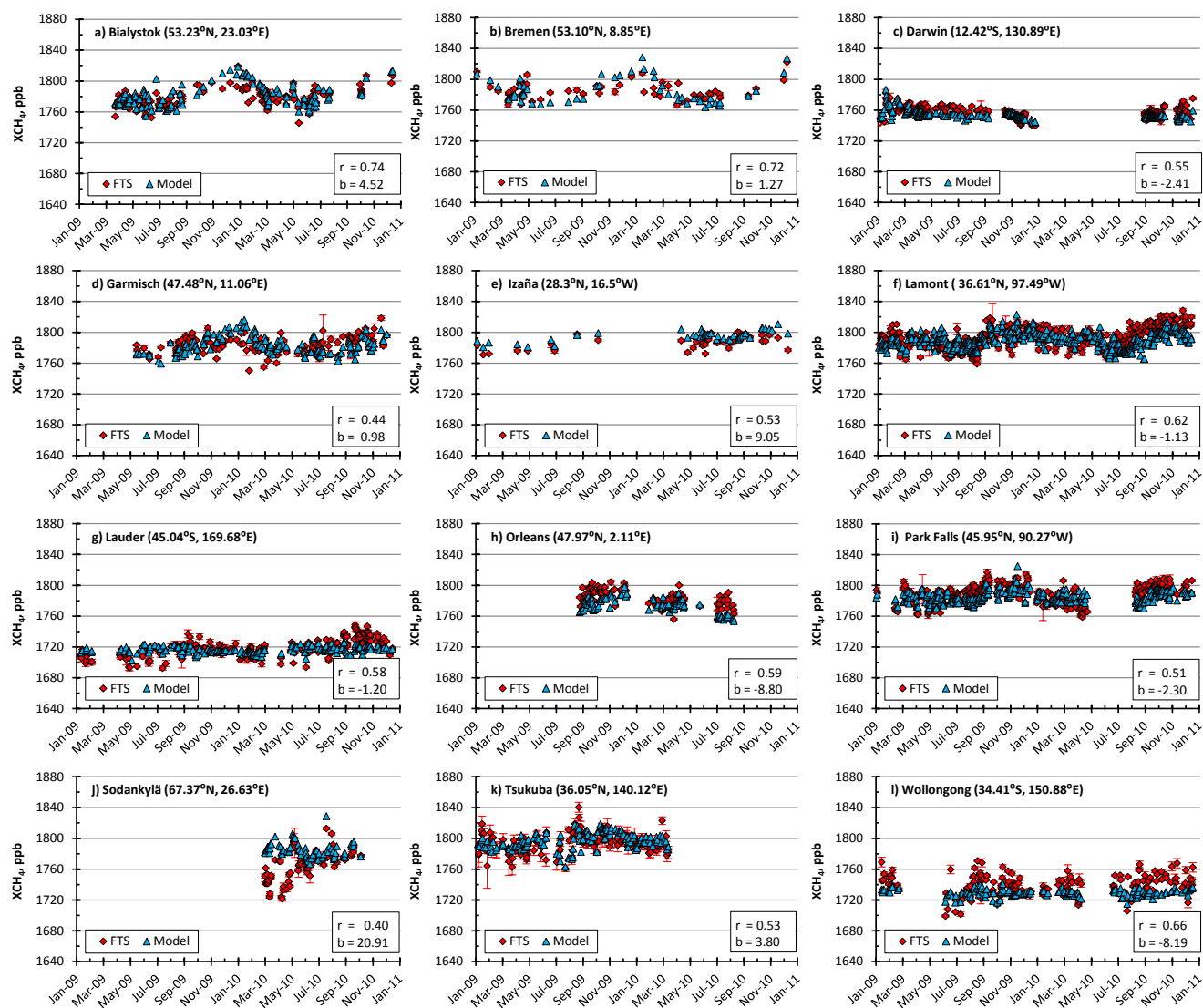


**Fig. 10.** Time series of XCH<sub>4</sub> measured by FTS and modelled by NIES TM for the period January 2009 to February 2011, for the following stations: (a) Bialystok (Poland, 53.22° N, 23.13° E); (b) Bremen (Germany, 53.10° N, 8.85° E); (c) Darwin (Australia, 12.42° S, 130.89° E); (d) Garmisch (Germany, 47.48° N, 11.06° E); (e) Izaña (Spain, 28.30° N, 16.50° W); (f) Lamont (USA, 36.6° N, 97.49° W); (g) Lauder (New Zealand, 45.04° S, 169.68° E); (h) Orleans (France, 47.97° N, 2.11° E); (i) Park Falls (USA, 45.95° N, 90.27° W); (j) Sodankylä (Finland, 67.37° N, 26.63° E); (k) Tsukuba (Japan, 36.05° N, 140.12° E); and (l) Wollongong (Australia, 34.41° S, 150.88° E). The “error” for each symbol is a combination of the spread due to weighted averaging within the 13:00 ± 1 h local time interval and observation error.

strong ( $> 0.85$ , Fig. 7). This is due to the fact that Pic Du Midi is a high altitude site (free troposphere) and Orleans a lowland site affected by near-surface small scale processes.

For Sodankylä, the comparison with the FTS data shows a relatively large bias ( $b = 20.91$  ppb) and low correlation coefficient ( $r = 0.40$ ), with larger mismatch in April. The bias may be caused by an overestimation of modelled CH<sub>4</sub> inside the polar vortex. Inside the vortex, the descent is much faster than in the zonal average and the stratospheric air with low concentrations of CH<sub>4</sub> drops to the troposphere. The ability of NIES TM to reproduce the observations in the vicinity of

the polar vortex is also limited due to horizontal grid resolution and a horizontal flux correction method implemented to NIES TM (Belikov et al., 2011). “Noise” appearing through the horizontal mass flux correction method may affect the vertical component of the wind vector and cause erroneously enhanced mixing and mass transport from the bottom of the atmosphere to the top (Belikov et al., 2011). In addition, NIES TM underestimates the age of air at high latitudes (Fig. 3c).

For Wollongong, the simulated results strongly underestimated the measurements (bias  $-11.05$  ppb), as the FTS’

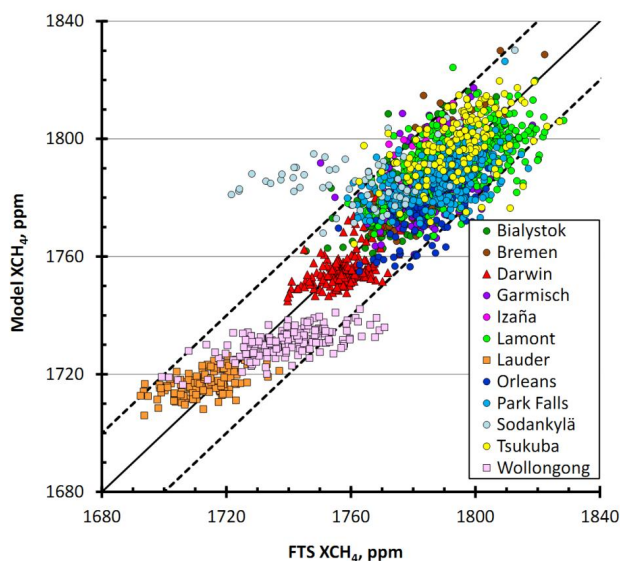


**Fig. 11.** Scatter diagram of modelled and FTS XCH<sub>4</sub> at all FTS sites. Dotted lines show a standard deviation of  $\pm 1\%$  of XCH<sub>4</sub>.

seasonal cycle amplitude was twice (Fig. 10l) the model value and twice that for other TCCON sites in the Southern Hemisphere. The reasons for this result remain unclear, although it may be relevant that Wollongong is located near major urban centers and sites of industrial activity, where emissions from coal mining are the largest source above background (Fraser et al., 2011).

The Izaña TCCON station is an oceanic site located on a small island and at high altitude ( $\sim 2$  km). The model's grid is too rough to reproduce local emission and loss, or capture the topography. The model is not able to reproduce small-scale variations in concentration, and this results in a weak correlation (0.53) and large bias (9.05 ppb).

In general, the minimum and maximum bias between the two datasets is  $-8.80$  ppb ( $-0.49\%$ ) and  $20.91$  ppb ( $1.16\%$ ), respectively. Figure 11 shows a scatter diagram of model XCH<sub>4</sub> data versus ground-based FTS XCH<sub>4</sub> data for 12 sites. The majority of points are within an interval of  $\pm 1\%$  of XCH<sub>4</sub>.

### 3.4.2 Modelled XCO<sub>2</sub> compared with TCCON FTS observations and GECM

We compared XCO<sub>2</sub> time-series with TCCON and constructed a 3-D CO<sub>2</sub> climatology GECM (Gap-filled and Ensemble Climatology Mean) (Saito et al., 2011) (Fig. 12). The seasonally varying climatology in GECM was estimated by taking an ensemble of the various transport models in combination with the interpolated bias correction, using a data product based on in situ measurements in the troposphere (GLOBALVIEW-CO<sub>2</sub>, 2010) and the monthly vertical and latitudinal distribution of the ACTM-derived mean age of air

in the stratosphere. Six transport models (ACTM, LMDZ4, NICAM, PCTM, and TM5), including the previous version of NIES TM (Belikov et al., 2011), participated in this study, but this is considered unlikely to seriously distort the results. The GECM seasonal cycle was nudged towards a seasonal cycle of the extended CO<sub>2</sub> record (GLOBALVIEW-CO<sub>2</sub>, 2010) by filtering out the inter-annual anomalies and the synoptic-scale variability in the extended CO<sub>2</sub> records using a curve-fitting procedure (Masarie and Tans, 1995).

The modelled XCO<sub>2</sub> and GECM XCO<sub>2</sub> time series show strong correlations with the TCCON data (correlation coefficients of 0.8–0.9; Table 3), as the seasonal XCO<sub>2</sub> variation is stronger than the XCH<sub>4</sub> cycle. Because of the use of actual meteorology and more up-to-date fluxes, the NIES TM described the seasonal variations slightly better for Bialystok, Bremen, Darwin, Lamont, Lauder, and Wollongong. Moreover, for all sites except Park Falls, Tsukuba, and Wollongong, the model bias was less than the bias for GECM. At other sites, comparisons of the model versus FTS and GECM versus FTS produced almost identical results.

The model shows quite good results in reproducing different seasonal cycles for all considered sites, including very steep decrease of XCO<sub>2</sub> at Sodankylä during the growing season and almost flat profiles at sites in the Southern Hemisphere. Figure 13 shows a scatter diagram of model XCO<sub>2</sub> data versus ground-based FTS XCO<sub>2</sub> data. The minimum and maximum differences in the model data compared with the FTS data are  $-0.62$  ppm ( $-0.16\%$ ) and  $1.21$  ppm ( $0.31\%$ ), respectively.

For XCO<sub>2</sub> there are several events with only one FTS measurement taken at approximately  $13:00 \pm 1$  h local time. Generally, the standard error in such cases is quite large especially for Lamont and Tsukuba (Fig. 12f, k).

## 4 Discussion

The model was able to reproduce the seasonal and inter-annual variability of XCO<sub>2</sub> and XCH<sub>4</sub> with correlation coefficients of 0.8–0.9 and 0.4–0.7, respectively. A small correlation was obtained for methane, due to the weak seasonal cycle of CH<sub>4</sub> and a high scatter of XCH<sub>4</sub> obtained from the ground FTS data within the selected interval ( $13:00 \pm 1$  h local time). The modelled time-series have quite small biases for all sites excluding Sodankylä, where model shows a large bias both for XCO<sub>2</sub> and XCH<sub>4</sub>,  $1.21$  ppm and  $20.91$  ppb, respectively. Moreover, GECM results also show a large bias ( $1.22$  ppm) for this site. Without Sodankylä's data, the model bias is  $\pm 0.2\%$  and  $\pm 0.5\%$  for XCO<sub>2</sub> and XCH<sub>4</sub>, respectively.

Model overestimation of CO<sub>2</sub> and CH<sub>4</sub> in the troposphere over Sodankylä during spring 2010 likely to be caused by errors in reproducing the polar vortex and requires further improvements in model parameterizations. Comparison with the other model simulations suggests the issue is not unique

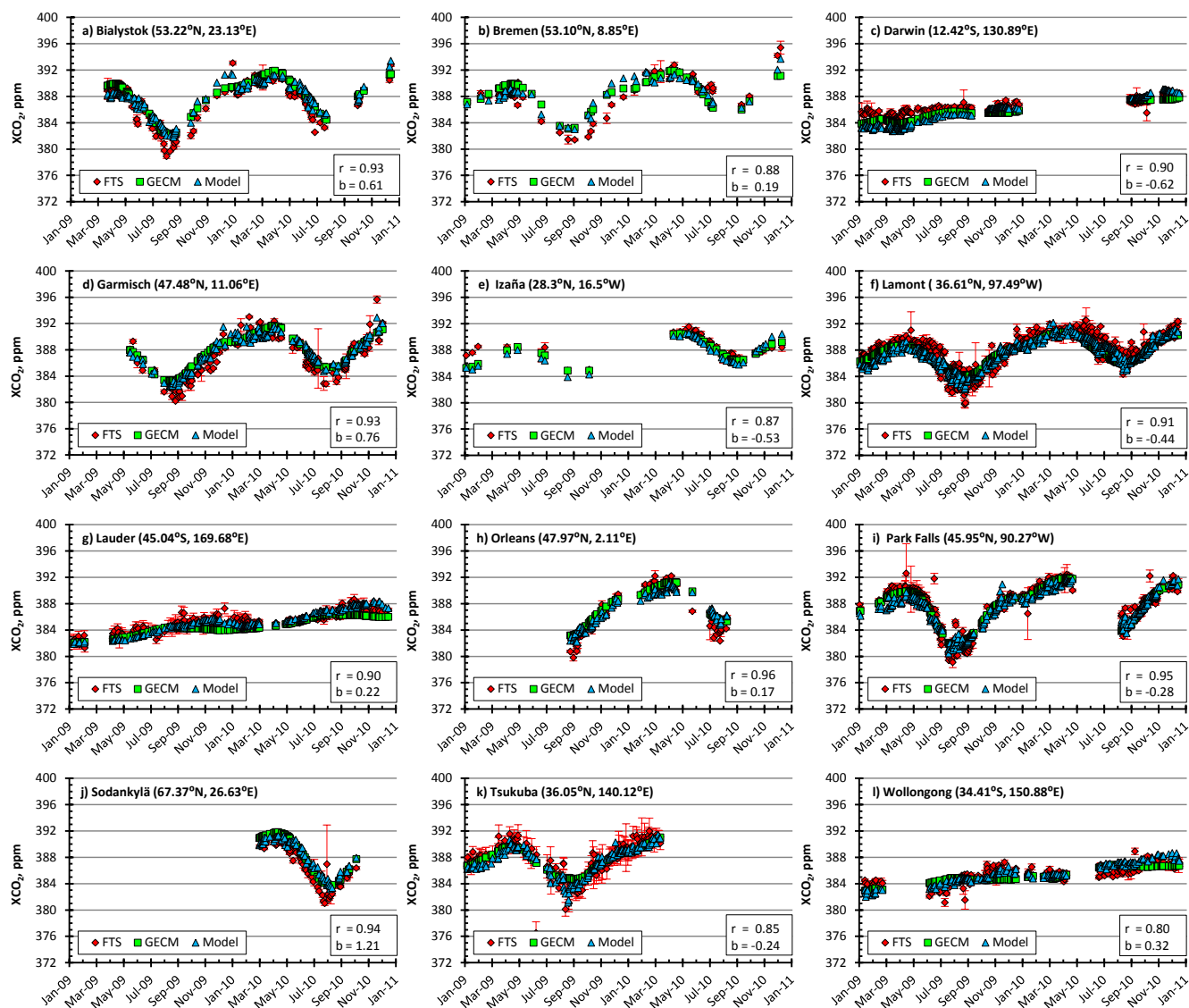


**Fig. 12.** Time series of XCO<sub>2</sub> measured by FTS, modelled by NIES TM and derived from a 3-D CO<sub>2</sub> climatology GECM for the period January 2009 to February 2011, for the following stations: (a) Bialystok (Poland, 53.22° N, 23.13° E); (b) Bremen (Germany, 53.10° N, 8.85° E); (c) Darwin (Australia, 12.42° S, 130.89° E); (d) Garmisch (Germany, 47.48° N, 11.06° E); (e) Izaña (Spain, 28.30° N, 16.50° W); (f) Lamont (USA, 36.6° N, 97.49° W); (g) Lauder (New Zealand, 45.04° S, 169.68° E); (h) Orleans (France, 47.97° N, 2.11° E); (i) Park Falls (USA, 45.95° N, 90.27° W); (j) Sodankylä (Finland, 67.37° N, 26.63° E); (k) Tsukuba (Japan, 36.05° N, 140.12° E); and (l) Wollongong (Australia, 34.41° S, 150.88° E). The “error” for each symbol is a combination of the spread due to weighted averaging within the 13:00 ±1 h local time interval and observation error.

for NIES TM and difficult to attribute just to the use of average descent/cooling rates to calculate vertical transport in the stratosphere, as for example the online ACTM model with frequent update of the radiative transport has also been shown to possess large biases between the observed and modeled XCH<sub>4</sub> (Saito et al., 2012).

The tracer column-averaged dry-air mole fraction is a sensitive indicator of overall model performance, because it is relatively unaffected by changes in vertical transport and sur-

face pressure, and shows minor spatial and temporal variations. As a result, the total column represents the model performance on a global scale. The XCO<sub>2</sub> and especially the XCH<sub>4</sub> scatter diagrams (Figs. 13 and 11, respectively) show balanced redistributions of tracer concentrations from the Northern Hemisphere, with high emissions to the Southern Hemisphere reproduced by the model. Moreover, the Darwin site shows vertical redistribution due to powerful tracer outflow from the PBL into the troposphere and the stratosphere,

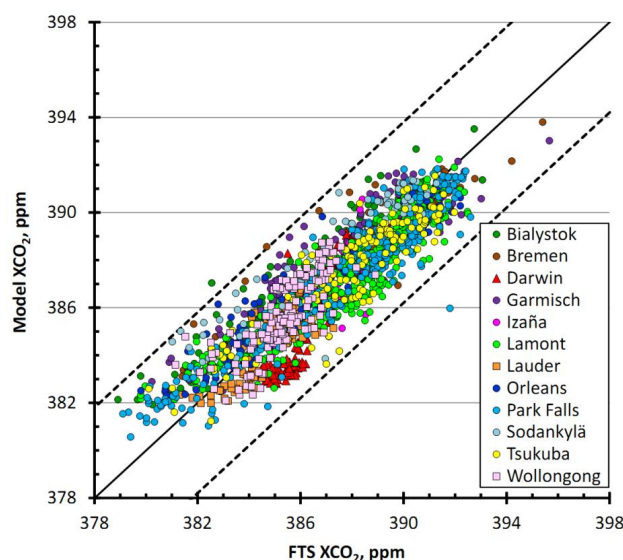


Fig. 13. As for Fig. 11, but for XCO<sub>2</sub>.

because this site is located in the tropics. The good agreement between simulated XCH<sub>4</sub> and FTS measurements highlights the ability of the model to capture the vertical profile of tracers, and in particular, to simulate balanced transport across the tropopause, as the mean age of methane was markedly different in the lower stratosphere and upper troposphere.

## 5 Conclusions

We performed multi-annual simulations of CO<sub>2</sub>, CH<sub>4</sub>, and SF<sub>6</sub> using the NIES three-dimensional offline chemical transport model (version NIES-08.1i), driven by JRA-25/JCDAS reanalysis data. This version uses a flexible hybrid sigma-isentropic ( $\sigma$ - $\theta$ ) vertical coordinate consisting of terrain-following and isentropic levels switched smoothly near the tropopause. Vertical transport in the isentropic part of the grid in the stratosphere was controlled by an air-ascending rate derived from the effective heating rate from JRA-25/JCDAS reanalysis, and was adjusted to fit the observed age of air in the stratosphere. The use of this vertical transport scheme avoided spurious vertical mixing caused by interpolation of the meteorological vertical wind component, and this resulted in improved model performance in the stratosphere, as the simulated vertical profiles of CO<sub>2</sub>, CH<sub>4</sub>, and SF<sub>6</sub> showed good agreement with balloon-borne observations. A comparison of model data with balloon-borne observations over Sanriku (Japan) in 2000–2007 revealed that the tracer transport simulations were performed with accuracies of  $\sim 5\%$  for CH<sub>4</sub> and SF<sub>6</sub>, and  $\sim 1\%$  for CO<sub>2</sub> compared with the observed VMRs.

We evaluated the model performance in simulating near-surface CH<sub>4</sub> concentrations by comparisons with measurements at GLOBALVIEW-CH<sub>4</sub> sites. In general, the model

was able to reproduce the variations in the surface concentrations more accurately ( $r = 0.6$ – $0.8$ ) at sites located some distance away from multiple emission sources. For other sites, where high emissions and local meteorology play a major role, it proved difficult to reproduce the CH<sub>4</sub> surface concentrations.

For measurements above 1 km, the model data are in good agreement with aircraft observations (1993–2007) over Surgut, West Siberia, which is an area with high emissions of methane from wetlands. However, the model was less effective in reproducing the high variability of CH<sub>4</sub> concentrations in the near-surface layer and did not simulate short-term variations with any reasonable accuracy. These results are in agreement with the findings of Houweling et al. (2010), and highlight the importance of obtaining a realistic representation of PBL dynamics, especially in regions with high tracer emissions.

Convolved with scene-dependent instrument averaging kernels, XCO<sub>2</sub> and XCH<sub>4</sub> were calculated from NIES TM tracer distributions and were compared with measurements acquired at TCCON ground-based FTS sites for the period from January 2009 to January 2011. The model was able to reproduce the seasonal and inter-annual variability of XCO<sub>2</sub> and XCH<sub>4</sub> with correlation coefficients of 0.8–0.9 and 0.4–0.8, respectively. A comparison of modelled data and TCCON observations revealed that the model biases are  $\pm 0.2\%$  for XCO<sub>2</sub> and  $\pm 0.5\%$  for XCH<sub>4</sub> without Sodankylä's data.

In general, the overall performance of NIES TM at TCCON sites is similar to the performance of four transport models (IFS, LMDZ, TM3, and TM5) compared by Houweling et al. (2010) for XCO<sub>2</sub> and to GEOS-Chem TM results published by Parker et al. (2011) for XCH<sub>4</sub>. Although the focus of future work will be to further improve and validate XCO<sub>2</sub> and XCH<sub>4</sub> simulations, the performance of the current model version is sufficient for use in evaluating satellite retrieval algorithms in areas not covered by ground-based FTS sites.

**Acknowledgements.** We thank T. Machida for aircraft observations of CH<sub>4</sub> over Surgut (Russia); and A. E. Andrews, T. M. Hall, and D. W. Waugh for providing observation data of the mean age of air in the stratosphere. We also thank P. K. Patra and the TransCom-CH<sub>4</sub> and CONTRAIL TMI communities for model setups, initial profiles, and emission fluxes used in the tracer transport simulation. We also thank S. Oshchepkov for insightful discussions and suggestions regarding the manuscript. The meteorological datasets used for this study were provided by the cooperative research project of the JRA-25/JCDAS long-term reanalysis by the Japan Meteorological Agency (JMA) and the Central Research Institute of Electric Power Industry (CRIEPI). We also thank GLOBALVIEW-CO<sub>2</sub>/CH<sub>4</sub> authors. For calculations, we used the computational resources of the NIES supercomputer system (NEC SX-8R/128M16).

TCCON data were obtained from the TCCON Data Archive, operated by the California Institute of Technology from the website at <http://tcon.ipac.caltech.edu/>. US funding for TCCON

comes from NASA's Terrestrial Ecology Program, grant number NNX11AG01G, the Orbiting Carbon Observatory Program, the Atmospheric CO<sub>2</sub> Observations from Space (ACOS) Program and the DOE/ARM Program. The Darwin TCCON site was built at Caltech with funding from the OCO project, and is operated by the University of Wollongong, with travel funds for maintenance and equipment costs funded by the OCO-2 project. We acknowledge funding to support Darwin and Wollongong from the Australian Research Council, Projects LE0669470, DP0879468, DP110103118 and LP0562346. Lauder TCCON measurements are funded by New Zealand Foundation of Research Science and Technology contracts C01X0204 and CO1X0406. We acknowledge financial support of the Bialystok and Orleans TCCON sites from the Senate of Bremen and EU projects IMECC and GEOMon, as well as maintenance and logistical work provided by AeroMeteo Service (Bialystok) and the RAMCES team at LSCE (Gif-sur-Yvette, France) and additional operational funding from the National Institute for Environmental Studies (NIES, Japan).

Edited by: P. Monks

## References

- Andrews, A. E., Boering, K. A., Daube, B. C., Wofsy, S. C., Loewenstein, M., Jost, H., Podolske, J. R., Webster, C. R., Herman, R. L., Scott, D. C., Flesch, G. J., Moyer, E. J., Elkins, J. W., Dutton, G. S., Hurst, D. F., Moore, F. L., Ray, E. A., Romashkin, P. A., and Strahan, S. E.: Mean ages of stratospheric air derived from in situ observations of CO<sub>2</sub>, CH<sub>4</sub>, and N<sub>2</sub>O, *J. Geophys. Res.*, 106, 32295–32314, doi:10.1029/2001JD000465, <http://www.agu.org/pubs/crossref/2001/2001JD000465.shtml>, 2001.
- Arakawa, A., and Moorthi, S.: Baroclinic instability in vertically discrete systems, *J. Atmos. Sci.*, 45, 1688–1707, 1988.
- Austin, P. M. and Houze Jr., R. A.: A technique for computing vertical transports by precipitating cumuli, *J. Atmos. Sci.*, 30, 1100–1111, 1973.
- Baker, D. F., Law, R. M., Gurney, K. R., Rayner, P., Peylin, P., Denning, A. S., Bousquet, P., Bruhwiler, L., Chen, Y.-H., Ciais, P., Fung, I. Y., Heimann, M., John, J., Maki, T., Maksyutov, S., Masarie, K., Prather, M., Pak, B., Taguchi, S., and Zhu, Z.: TransCom 3 inversion intercomparison: Impact of transport model errors on the interannual variability of regional CO<sub>2</sub> fluxes 1988–2003, *Global Biogeochem. Cy.*, 20, GB1002, doi:10.1029/2004GB002439, 2006.
- Belikov, D., Maksyutov, S., Miyasaka, T., Saeki, T., Zhuravlev, R., and Kiryushov, B.: Mass-conserving tracer transport modelling on a reduced latitude-longitude grid with NIES-TM, *Geosci. Model Dev.*, 4, 207–222, doi:10.5194/gmd-4-207-2011, 2011.
- Bergamaschi, P., Frankenberg, C., Meirink, J. F., Krol, M., Dentener, F., Wagner, T., Platt, Y., Kaplan, J. O., Kroner, S., Heimann, M., Dlugokencky, E. J., and Goede, A.: Satellite cartography of atmospheric methane from SCIAMACHY on board ENVISAT: 2. Evaluation based on inverse model simulations, *J. Geophys. Res.*, 112, D02304, doi:10.1029/2006JD007268, 2007.
- Bergamaschi, P., Frankenberg, C., Meirink, J. F., Krol, M., Villani, M. G., Houweling, S., Dentener, F., Dlugokencky, E. J., Miller, J. B., Gatti, L. V., Engel, A., and Levin, I.: Inverse modeling of global and regional CH<sub>4</sub> emissions using SCIAMACHY satellite retrievals, *J. Geophys. Res.*, 114, D22301, doi:10.1029/2009JD012287, 2009.
- Bloom, A. A., Palmer, P. I., Fraser, A., David, S. R., and Frankenberg C.: Large-scale controls of methanogenesis inferred from methane and gravity space-borne data, *Science*, 327, 322–325, doi:10.1126/science.1175176, 2010.
- Bleck, R.: On the use of hybrid vertical coordinates in numerical weather prediction models, *Mon. Wea. Rev.*, 106, 1233–1244, 1978.
- Boden, T. A., Marland, G., and Andres, R. J.: Global, Regional, and National Fossil Fuel CO<sub>2</sub> Emissions, Carbon Dioxide Information Analysis Center, Oak Ridge National Laboratory, U.S. Department of Energy, Oak Ridge, Tenn, USA, doi:10.3334/CDIAC/00001, 2009.
- Boering, K. A., Wofsy, S. C., Daube, B. C., Schneider, H. R., Loewenstein, M., and Podolske, J. R.: Stratospheric transport rates and mean age distribution derived from observations of atmospheric CO<sub>2</sub> and N<sub>2</sub>O, *Science*, 274, 1340–1343, 1996.
- Bousquet, P., Ciais, P., Miller, J. B., Dlugokencky, E. J., Hauglustaine, D. A., Prigent, C., van der Werf, G. R., Peylin, P., Brunke, E.-G., Carouge, C., Langenfelds, R. L., Lathiere, J., Papa, F., Ramonet, M., Schmidt, M., Steele, L. P., Tyler, S. C., and White, J.: Contribution of anthropogenic and natural sources to atmospheric methane variability, *Nature*, 443, 439–443, doi:10.1038/nature05132, 2006.
- Butz, A., Guerlet, S., Hasekamp, O., Schepers, D., Galli, A., Aben, I., Frankenberg, C., Hartmann, J. -M., Tran, H., Kuze, A., Keppel-Aleks, G., Toon, G., Wunch, D., Wennberg, P., Deutscher, N., Griffith, D., Messerschmidt, J., Macatangay, R., Notholt, J., and Warneke, T.: Toward accurate CO<sub>2</sub> and CH<sub>4</sub> observations from GOSAT, *Geophys. Res. Lett.*, 38, L14812, doi:10.1029/2011GL047888, 2011.
- Bovensmann, H., Burrows, J. P., Buchwitz, M., Frerick, J., Noël, S., Rozanov, V. V., Chance, K. V., and Goede, A. H. P.: SCIAMACHY – Mission objectives and measurement modes, *J. Atmos. Sci.*, 56, 127–150, 1999.
- Chipperfield, M. P.: New Version of the TOMCAT/SLIMCAT Off-Line Chemical Transport Model: Intercomparison of Stratospheric Tracer Experiments, *Q. J. R. Meteorol. Soc.*, 132, 1179–1203, doi:10.1256/qj.05.51, 2006.
- Connor, B. J., Boesch, H., Toon, G., Sen, B., Miller, C., and Crisp, D.: Orbiting Carbon Observatory: Inverse method and prospective error analysis, *J. Geophys. Res.*, 113, D05305, doi:10.1029/2006JD008336, 2008.
- Conway T. and Tans, P.: NOAA/ESRL ([www.esrl.noaa.gov/gmd/ccgg/trends/](http://www.esrl.noaa.gov/gmd/ccgg/trends/)), 2011.
- Conway, T. J., Tans, P. P., Waterman, L. S., Thoning, K. W., Kitzis, D. R., Masarie, K. A., and Zhang, N.: Evidence for interannual variability of the carbon cycle from the National Oceanic and Atmospheric Administration/Climate Monitoring and Diagnostics Laboratory Global Air Sampling Network, *J. Geophys. Res.*, 99, 22831–22855, doi:10.1029/94JD01951, 1994.
- Crisp, D., Fisher, B. M., O'Dell, C., Frankenberg, C., Basilio, R., Bösch, H., Brown, L. R., Castano, R., Connor, B., Deutscher, N. M., Eldering, A., Griffith, D., Gunson, M., Kuze, A., Mandrake, L., McDuffie, J., Messerschmidt, J., Miller, C. E., Morino, I., Natraj, V., Notholt, J., O'Brien, D. M., Oyafuso, F., Polonsky, I., Robinson, J., Salawitch, R., Sherlock, V., Smyth, M., Suto,

- H., Taylor, T. E., Thompson, D. R., Wennberg, P. O., Wunch, D., and Yung, Y. L.: The ACOS CO<sub>2</sub> retrieval algorithm – Part II: Global X<sub>CO<sub>2</sub></sub> data characterization, *Atmos. Meas. Tech.*, 5, 687–707, doi:10.5194/amt-5-687-2012, 2012.
- Douglass, A. R., Prather, M. J., Hall, T. M., Strahan, S. E., Rasch, P. J., Sparling, L. C., Coy, L., and Rodriguez J. M.: Choosing meteorological input for the global modeling initiative assessment of high-speed aircraft, *J. Geophys. Res.*, 104, 27545–27564, 1999.
- Denning, A. S., Randall, D. A., Collatz, G. J., and Sellers, P. J.: Simulations of terrestrial carbon metabolism and atmospheric CO<sub>2</sub> in a general circulation model. II. Simulated CO<sub>2</sub> concentrations, *Tellus B Chem. Phys. Meteorol.*, 48, 543–567, doi:10.1034/j.1600-0889.1996.t01-1-00010.x, 1996
- Eguchi, N., Saito, R., Saeki, T., Nakatsuka, Y., Belikov, D., and Maksyutov S.: A priori covariance estimation for CO<sub>2</sub> and CH<sub>4</sub> retrievals, *J. Geophys. Res.*, 115, D10215, doi:10.1029/2009JD013269, 2010.
- Eliassen, A. and Raustein, E.: A numerical integration experiment with a model atmosphere based on isentropic coordinates, *Meteorologische Annaler*, 5, 45–63, 1968.
- Elkins, J. W., Fahey, D. W., Gilligan, J. M., Dutton, G. S., Baring, T. J., Volk, C. M., Dunn, R. E., Myers, R. C., Montzka, S. A., Wamsley, P. R., Hayden, A. H., Butler, J. H., Thompson, T. M., Swanson, T. H., Dlugokencky, E. J., Novelli, P. C., Hurst, D. F., Lobert, J. M., Ciciora, S. J., McLaughlin, R. J., Thompson, T. L., Winkler, R. H., Fraser, P. J., Steele, L. P., and Lucarelli, M. P.: Airborne gas chromatograph for in situ measurements of long lived species in the upper troposphere and lower stratosphere, *Geophys. Res. Lett.*, 23, 347–350, 1996
- Eluszkiewicz, J., Helmer, R. S., Mahlman, J. D., Bruhwiler, L., and Takacs, L. L.: Sensitivity of age-of-air calculations to the choice of advection scheme, *J. Atmos. Sci.*, 57, 3185–3201, 2000.
- Engel, A., Möbius, T., Bönišch, H., Schmidt, U., Heinz, R., Levin, I., Atlas, E., Aoki, S., Nakazawa, T., Sugawara, S., Moore, F., Hurst, D., Elkins, J., Schauffler, S., Andrews, A., Boering, K.: Age of stratospheric air unchanged within uncertainties over the past 30 years, *Nat. Geosci.*, 2, 28–31, doi:10.1038/ngeo388, 2009.
- Feichter, J. and Crutzen, P. J.: Parameterization of vertical transport due to deep cumulus convection in a global transport model and its evaluation with <sup>222</sup>Rn measurements, *Tellus B*, 42, 100–117, 1990.
- Folkens, I., Loewenstein, M., Podolske, J., Oltmans, S. J., and Profitt, M.: A barrier to vertical mixing at 14 km in the tropics: Evidence from ozone sondes and aircraft measurements, *J. Geophys. Res.*, 104, 22, 095–22, 102, 1999.
- Fraser, A., Chan Miller, C., Palmer, P. I., Deutscher, N. M., Jones, N. B., and Griffith D. W. T.: The Australian methane budget: Interpreting surface and train-borne measurements using a chemistry transport model, *J. Geophys. Res.*, 116, D20306, doi:10.1029/2011JD015964, 2011.
- Fueglistaler, S., Legras, B., Beljaars, A., Morcrette, J. J., Simmons, A., Tompkins, A. M., and Uppala, S.: The diabatic heat budget of the upper troposphere and lower/mid stratosphere in ECMWF reanalysis, *Q. J. Roy. Meteor. Soc.*, 135, 21–37, 2009.
- Gettelman, A., de Fujiwara, P. M., Fu, Q., Voemel, H., Gohar, L. K., Johanson, C., and Ammeraman, M.: Radiation balance of the tropical tropopause layer, *J. Geophys. Res.*, 109, D07103, doi:10.1029/2003JD004190, 2004.
- GLOBALVIEW-CH4: Cooperative Atmospheric Data Integration Project – Methane. CD-ROM, NOAA ESRL, Boulder, Colorado, also available at: ftp.cmdl.noaa.gov/Path:ccg/ch4/GLOBALVIEW, 2009.
- GLOBALVIEW-CO2: Cooperative Atmospheric Data Integration Project – Carbon Dioxide. CD-ROM, NOAA ESRL, Boulder, Colorado, also available at: ftp.cmdl.noaa.gov/Path:ccg/co2/GLOBALVIEW, 2010.
- Grell, G. A.: Prognostic evaluation of assumptions used by cumulus parameterizations, *Mon. Weather Rev.*, 121, 764–787, 1993.
- Gurney, K. R., Law, R. M., Denning, A. S., Rayner, P. J., Pak, B. C., Baker, D., Bousquet, P., Bruhwiler, L., Chen, Y. H., Ciais, P., Fung, I. Y., Heimann, M., John, J., Maki, T., Maksyutov, S., Peylin, P., Prather, M., and Taguchi, S.: Transcom 3 inversion intercomparison: Model mean results for the estimation of seasonal carbon sources and sinks, *Global Biogeochem. Cy.*, 18, GB1010, doi:10.1029/2003GB002111, 2004.
- Hack, J. J., Boville, B. A., Briegleb, B. P., Kiehl, J. T., Rasch, P. J., and Williamson, D. L.: Description of the NCAR community climate model (CCM2), NCAR/TN-382, 108, 1993.
- Hall, T. M., Waugh, D. W., Boering, K. A., and Plumb R. A.: Evaluation of transport in stratospheric models, *J. Geophys. Res.*, 104, 18815–18839, 1999.
- Harnisch, J., Borchers, R., Fabian, P., and Maiss M.: CF<sub>4</sub> and the age of mesospheric and polar vortex air, *Geophys. Res. Lett.*, 26, 295–298, 1999.
- Houweling, S., Aben, I., Breon, F.-M., Chevallier, F., Deutscher, N., Engelen, R., Gerbig, C., Griffith, D., Hungershofer, K., Macatangay, R., Marshall, J., Notholt, J., Peters, W., and Serrar, S.: The importance of transport model uncertainties for the estimation of CO<sub>2</sub> sources and sinks using satellite measurements, *Atmos. Chem. Phys.*, 10, 9981–9992, doi:10.5194/acp-10-9981-2010, 2010.
- Hsu, Y.-J. G. and Arakawa, A.: Numerical modeling of the atmosphere with an isentropic vertical coordinate, *Mon. Wea. Rev.*, 118, 1933–1959, 1990.
- Ingmann, P.: A-SCOPE, Advanced space carbon and climate observation of planet earth, Report for Assessment, SP-1313/1, ESA communication production office, Noordwijk, The Netherlands, 2009.
- Intergovernmental Panel on Climate Change (IPCC), Climate change 2007: The Physical Science Basis: Contribution of Working Group I to the Fourth Assessment Report of the Intergovernmental Panel on Climate Change, edited by: Solomon, S., Qin, D., Manning, M., Chen, Z., Marquis, M., Averyt, K. B., Tignor, M., and Miller, H. L., Cambridge University Press, Cambridge, UK and New York, NY, USA, 996 pp., 2007.
- Kalnay, E.: Atmospheric Modeling, Data Assimilation and Predictability, Cambridge University Press, 364 (ISBN-10: 0521796296, ISBN-13: 978-0521796293), 2002.
- Keppel-Aleks, G., Wennberg, P. O., and Schneider, T.: Sources of variations in total column carbon dioxide, *Atmos. Chem. Phys.*, 11, 3581–3593, doi:10.5194/acp-11-3581-2011, 2011.
- Konopka, P., Günther, G., Müller, R., dos Santos, F. H. S., Schiller, C., Ravegnani, F., Ulanovsky, A., Schlager, H., Volk, C. M., Viciani, S., Pan, L. L., McKenna, D.-S., and Riese, M.: Contribution of mixing to upward transport across the tropical tropopause layer (TTL), *Atmos. Chem. Phys.*, 7, 3285–3308, doi:10.5194/acp-7-3285-2007, 2007.

- Konor, C. S. and Arakawa, A.: Design of an atmospheric model based on a generalized vertical coordinate, *Mon. Weather Rev.*, 125, 1649–1673, 1997.
- Levin, I., Naegler, T., Heinz, R., Osusko, D., Cuevas, E., Engel, A., Imberger, J., Langenfelds, R. L., Neininger, B., Rohden, C. V., Steele, L. P., Weller, R., Worthy, D. E., and Zimov, S. A.: The global SF<sub>6</sub> source inferred from long-term high precision atmospheric measurements and its comparison with emission inventories, *Atmos. Chem. Phys.*, 10, 2655–2662, doi:10.5194/acp-10-2655-2010, 2010.
- Mahowald, N. M., Plumb, R. A., Rasch, P. J., del Corral, J., and Sassi, F.: Stratospheric transport in a three-dimensional isentropic coordinate model, *J. Geophys. Res.*, 107, 4254, doi:10.1029/2001JD001313, 2002.
- Maiss, M., Steele, L. P., Francey, R. J., Fraser, P. J., Langenfelds, R. L., Trivett, N. B. A. and Levin, I.: Sulfur hexafluoride – a powerful new atmospheric tracer, *Atmos. Environ.*, 30, 1621–1629, 1996.
- Maksyutov, S., Patra, P. K., Onishi, R., Saeki, T., and Nakazawa, T.: NIES/FRCGC global atmospheric tracer transport model: description, validation, and surface sources and sinks inversion, *J. Earth Simulator*, 9, 3–18, 2008.
- Masarie, K.A. and Tans P. P.: Extension and integration of atmospheric carbon dioxide data into a globally consistent measurement record, *J. Geophys. Res.*, 100, 11593–11610, 1995.
- Meirink, J. F., Eskes, H. J., and Goede, A. P. H.: Sensitivity analysis of methane emissions derived from SCIAMACHY observations through inverse modelling, *Atmos. Chem. Phys.*, 6, 1275–1292, doi:10.5194/acp-6-1275-2006, 2006.
- Miyazaki, K., Patra, P. K., Takigawa, M., Iwasaki, T., and Nakazawa, T.: Global-scale transport of carbon dioxide in the troposphere, *J. Geophys. Res.*, 113, D15301, doi:10.1029/2007JD009557, 2008.
- Monge-Sanz, B. M., Chipperfield, M. P., Simmons, A. J., and Upala S. M.: Mean age of air and transport in a CTM: Comparison of different ECMWF analyses, *Geophys. Res. Lett.*, 34, L04801, doi:10.1029/2006GL028515, 2007.
- Morino, I., Uchino, O., Inoue, M., Yoshida, Y., Yokota, T., Wennberg, P.O., Toon, G.C., Wunch, D., Roehl, C.M., Notholt, J., Warneke, T., Messerschmidt, J., Griffith, D.W. T., Deutscher, N.M., Sherlock, V., Connor, B., Robinson, J., Sussmann, R., and Rettinger, M.: Preliminary validation of column-averaged volume mixing ratios of carbon dioxide and methane retrieved from GOSAT short-wavelength infrared spectra, *Atmos. Meas. Tech.*, 4, 1061–1076, doi:10.5194/amt-4-1061-2011, 2011.
- Nakazawa T., Aoki, S., Kawamura, K., Saeki, T., Sugawara, S., Honda, H., Hashida, G., Morimoto, S., Yoshida, N., Toyoda, S., Makide, Y., Shirai, T.: Variations of stratospheric trace gases measured using a balloon-borne cryogenic sampler, *Adv. Space Res.*, 30, 5, 1349–1357, ISSN 0273-1177, doi:10.1016/S0273-1177(02)00551-3, 2002.
- Niwa, Y., Patra, P. K., Sawa, Y., Machida, T., Matsueda, H., Belikov, D., Maki, T., Ikegami, M., Imasu, R., Maksyutov, S., Oda, T., Satoh, M., and Takigawa, M.: Three-dimensional variations of atmospheric CO<sub>2</sub>: aircraft measurements and multi-transport model simulations, *Atmos. Chem. Phys.*, 11, 13359–13375, doi:10.5194/acp-11-13359-2011, 2011.
- Olivier, J. G. J. and Berdowski, J. J. M.: Global emissions sources and sinks, A.A. Balkema Publishers/Swets and Zeitlinger Publishers, Lisse, The Netherlands, 2001.
- Onogi, K., Tsutsui, J., Koide, H., Sakamoto, M., Kobayashi, S., Hatushika, H., Matsumoto, T., Yamazaki, N., Kamahori, H., Takahashi, K., Kadokura, S., Wada, K., Kato, K., Oyama, R., Ose, T., Mannoji, N., and Taira, R.: The JRA-25 Reanalysis, *J. Met. Soc. Jap.*, 85, 369–432, 2007.
- Parker, R., Boesch, H., Cogan, A., Fraser, A., Feng, L., Palmer, P.I., Messerschmidt, J., Deutscher, N., Griffith, D. W. T., Notholt, J., Wennberg, P.O., and Wunch, D.: Methane observations from the Greenhouse Gases Observing SATellite: Comparison to ground-based TCCON data and model calculations, *Geophys. Res. Lett.*, 38, L15807, doi:10.1029/2011GL047871, 2011.
- Patra, P. K., Houweling, S., Krol, M., Bousquet, P., Belikov, D., Bergmann, D., Bian, H., Cameron-Smith, P., Chipperfield, M. P., Corbin, K., Fortems-Cheiney, A., Fraser, A., Gloor, E., Hess, P., Ito, A., Kawa, S. R., Law, R. M., Loh, Z., Maksyutov, S., Meng, L., Palmer, P. I., Prinn, R. G., Rigby, M., Saito, R., and Wilson, C.: TransCom model simulations of CH<sub>4</sub> and related species: linking transport, surface flux and chemical loss with CH<sub>4</sub> variability in the troposphere and lower stratosphere, *Atmos. Chem. Phys.*, 11, 12813–12837, doi:10.5194/acp-11-12813-2011, 2011.
- Plumb, R. A. and Ko, M. K. W.: Interrelationships between mixing ratios of long-lived stratospheric constituents, *J. Geophys. Res.*, 97, 10145–10156, 1992.
- Rayner, P. J. and O'Brien D. M.: The utility of remotely sensed CO<sub>2</sub> concentration data in surface source inversions, *Geophys. Res. Lett.*, 28, 175–178, 2001.
- Ray, E. A., Moore, F. L., Elkins, J. W., Dutton, G. S., Fahey, D. W., Vömel, H., Oltmans, S. J., and Rosenlof, K. H.: Transport into the Northern Hemisphere lowermost stratosphere revealed by in situ tracer measurements, *J. Geophys. Res.*, 104, 26565–26580, 1999.
- Rodgers, C. D. and Connor, B. J.: Intercomparison of remote sounding instruments. *J. Geophys. Res.* 108, 4116–4229, doi:10.1029/2002JD002299, 2003.
- Rohs, S., Schiller, C., Riese, M., Engel, A., Schmidt, U., Wetter, T., Levin, I., Nakazawa, T., Aoki, S.: Long-term changes of methane and hydrogen in the stratosphere in the period 1978–2003, *J. Geophys. Res.*, 111, D14315, doi:10.1029/2005JD006877, 2006.
- Saito R., Houweling, S., Patra, P.K., Belikov, D., Lokupitiya, R., Niwa, Y., Chevallier, F., Saeki, T., and Maksyutov S.: TransCom satellite intercomparison experiment: Construction of a bias corrected atmospheric CO<sub>2</sub> climatology, *J. Geophys. Res.*, 116, D21120, doi:10.1029/2011JD016033, 2011.
- Saito, R., Patra, P. K., Deutscher, N., Wunch, D., Ishijima, K., Sherlock, V., Blumenstock, T., Dohe, S., Griffith, D., Hase, F., Heikkinen, P., Kyrö, E., Macatangay, R., Mendonca, J., Messerschmidt, J., Morino, I., Notholt, J., Rettinger, M., Strong, K., Sussmann, R., and Warneke, T.: Technical Note: Latitude-time variations of atmospheric column-average dry air mole fractions of CO<sub>2</sub>, CH<sub>4</sub> and N<sub>2</sub>O, *Atmos. Chem. Phys.*, 12, 7767–7777, doi:10.5194/acp-12-7767-2012, 2012.
- Sherwood, S. C. and Dessler, A. E.: Convective mixing near the tropopause: Insights from seasonal variations, *J. Atmos. Sci.*, 60, 2674–2685, 2003.
- Stiller, G. P., von Clarmann, T., Höpfner, M., Glatthor, N., Grabowski, U., Kellmann, S., Kleinert, A., Linden, A., Milz, M., Reddman, T., Steck, T., Fischer, H., Funke, B., López-Puertas, M., and Engel, A.: Global distribution of mean age

- of stratospheric air from MIPAS SF<sub>6</sub> measurements, *Atmos. Chem. Phys. Discuss.*, 7, 13653–13697, doi:10.5194/acpd-7-13653-2007, 2007.
- Tiedtke, M.: A comprehensive mass flux scheme for cumulus parameterization in large scale models, *Mon. Weather Rev.*, 117, 1779–1800, 1989.
- Thuburn, J. and Craig, G. C.: On the temperature structure of the tropical stratosphere, *J. Geophys. Res.*, 107, 4017, doi:10.1029/2001JD000448, 2002.
- Washenfelder, R. A., Wennberg, P. O., and Toon, G. C.: Tropospheric methane retrieved from ground-based near-IR solar absorption spectra, *Geophys. Res. Lett.*, 30, 2226, doi:10.1029/2003GL017969, 2003.
- Waugh, D. W., and Hall, T. M.: Age of stratospheric air: Theory, observations, and models, *Rev. Geophys.*, 40, doi:10.1029/2000RG000101, 2002.
- Weaver, C. J., Douglass, A. R., and Rood, R. B.: Thermodynamic balance of three-dimensional stratospheric winds derived from a data assimilation procedure, *J. Atmos. Sci.*, 50, 2987–2993, 1993.
- Wunch, D., Toon, G. C., Wennberg, P. O., Wofsy, S. C., Stephens, B. B., Fischer, M. L., Uchino, O., Abshire, J. B., Bernath, P., Biraud, S. C., Blavier, J.-F. L., Boone, C., Bowman, K. P., Browell, E. V., Campos, T., Connor, B. J., Daube, B. C., Deutscher, N. M., Diao, M., Elkins, J. W., Gerbig, C., Gottlieb, E., Griffith, D. W. T., Hurst, D. F., Jimenez, R., Keppel-Aleks, G., Kort, E. A., Macatangay, R., Machida, T., Matsueda, H., Moore, F., Morino, I., Park, S., Robinson, J., Roehl, C. M., Sawa, Y., Sherlock, V., Sweeney, C., Tanaka, T., and Zondlo, M. A.: Calibration of the Total Carbon Column Observing Network using aircraft profile data, *Atmos. Meas. Tech.*, 3, 1351–1362, doi:10.5194/amt-3-1351-2010, 2010.
- Wunch, D., Toon, G., Blavier, J.-F. L., Washenfelder, R. A., Notholt, J., Connor, B. J., Griffith, D. W. T., Sherlock, V., and Wennberg, P. O.: The Total Carbon Column Observing Network (TCCON), *Phil. Trans. R. Soc. A369*, 2087–2112, doi:10.1098/rsta.2010.0240, 2011.
- Yang, Z., Washenfelder, R. A., Keppel-Aleks, G., Krakauer, N. Y., Randerson, J. T., Tans, P. P., Sweeney, C., and Wennberg, P. O.: New constraints on Northern Hemisphere growing season net flux, *Geophys. Res. Lett.*, 34, 1–6, doi:10.1029/2007GL029742, 2007.
- Yokota, T., Yoshida, Y., Eguchi, N., Ota, Y., Tanaka, T., Watanabe, H., and Maksyutov, S.: Global concentrations of CO<sub>2</sub> and CH<sub>4</sub> retrieved from GOSAT: First preliminary results, *Scientific Online Letters on the Atmosphere (SOLA)*, 5, 160–163, doi:10.2151/sola.2009-041, 2009.
- Zhuang, Q., Melack, J. M., Zimov, S., Walter, K. M., Butenhoff, C. L., and Khalil, M. A. K.: Global methane emissions from wetlands, rice paddies, and lakes, *Eos*, 90, 37–38, 2009.